Kinematical Distributions of Neutrino-Produced Lepton Triplets*

Jørgen Løvseth† and Mark Radomski‡
Institute of Theoretical Physics, Department of Physics, Stanford University, Stanford, California 94305
(Received 19 January 1971)

Differential distributions in lepton triplets $\nu_\mu\mu^-\mu^+$, $\nu_e\mu^-e^+$, $\nu_e e^-e^+$ produced from neutrinos through the point four-fermion interaction and single-photon exchange with a nuclear target have been calculated using a Monte Carlo method. These are fundamental processes which can be calculated to arbitrary accuracy, and which test aspects of the leptonic weak interactions, in particular diagonal processes, which are not accessible to other tests. The calculations cover energies from 1.5 to 40 GeV, and targets of mass 1, 12, 56, and 208. Salient features of the results are that typically the negative lepton is energetic, the positive one much less energetic, and transverse momenta of the charged leptons are quite large (100–200 MeV/c at 15 GeV).

I. INTRODUCTION

We shall discuss the processes

$$\begin{aligned}&\text{(a)}\ \ \nu_\mu + Z \to Z + \mu^- + \mu^+ + \nu_\mu\,,\\ &\text{(b)}\ \ \nu_\mu + Z \to Z + \mu^- + e^+ + \nu_e\,,\\ &\text{(c)}\ \ \nu_e + Z \to Z + e^- + e^+ + \nu_e\,,\\ &\text{(d)}\ \ \nu_e + Z \to Z + e^- + \mu^+ + \nu_\mu\,,\end{aligned} \tag{1}$$

where Z indicates that production takes place in the Coulomb field of a nucleus or nucleon of charge Ze.

Czyz, Sheppey, and Walecka[1] have discussed these processes earlier and stressed their importance as a testing ground for the theory of weak interactions. They calculated the total cross sections and could then use some tricks to simplify the trace calculations and phase-space integrations involved. They also showed that the cross sections are unchanged if the leptons are replaced by their antiparticles.

Of the four processes (1), (d) is least interesting because it is nondiagonal (see below) and difficult to observe (requiring an incoming electron neutrino). We consider only the first three processes to have practical interest, and our purpose is to calculate characteristic kinematical spectra of the charged lepton pair. We base our calculations on the Fermi point interaction described by the phenomenological interaction Lagrangian

$$\mathfrak{L}_i = \frac{G}{\sqrt{2}}(J_\alpha + j_\alpha)^\dagger (J_\alpha + j_\alpha)\,, \tag{2}$$

where G is the Fermi constant, given in terms of the proton mass as

$$G = 1.01\times 10^{-5}/M_p^{\,2}\,. \tag{3}$$

J_α is the hadronic weak current, which does not contribute in our case, and j_α is the lepton current, given as

$$j_\alpha = \bar\psi_e\, i\gamma_\alpha(1+\gamma_5)\psi_{\nu_e} + \bar\psi_\mu\, i\gamma_\alpha(1+\gamma_5)\psi_{\nu_\mu}\,, \tag{4}$$

where the ψ's are the lepton field operators, and the γ's the usual Dirac matrices. [We use a metric where $a = (\vec{a}, ia_0)$ and γ matrices which are Hermitian, satisfying $\gamma_\alpha\gamma_\beta + \gamma_\beta\gamma_\alpha = 2\delta_{\alpha\beta}$.]

Equations (2)–(4) together with the usual electromagnetic interactions give a unique prediction for these processes, which, together with muon decay and neutrino scattering on electrons, probably constitute the only possibilities available in practice to study four-lepton interactions where no form factors enter at the weak vertex to obscure the picture. Reactions (1) are, however, the only ones which have an off-mass-shell lepton entering the weak vertex, allowing, in principle, more information to be extracted. They also provide greater momentum transfers than neutrino-electron scattering and especially muon decay.

Gell-Mann, Goldberger, Kroll, and Low[2] have caused a revival of interest in these types of reactions by proposing a class of theories for weak interactions wherein the well-known divergence problems of the higher orders appear only in what they call diagonal interactions, which operate between particle pairs of the same type, e.g., $(\bar e\nu_e)(\bar\nu_e e)$, $(\bar\mu\nu_\mu)(\bar\nu_\mu\mu)$, etc.

One way to realize such a theory is to have a set of vector mesons of mass M_W with propagators

$$(\delta_{\alpha\beta} + k_\alpha k_\beta/M_W^{\,2})/(M_W^{\,2} + k^2) \tag{5}$$

and a second set of gradient-coupled spin-zero mesons of mass μ with effective propagators

$$k_\alpha k_\beta/(\mu^2 + k^2)\,,$$

where k is the momentum transfer. Couplings can then be so arranged that the divergent parts (stemming from the terms $k_\alpha k_\beta$) cancel as $k\to\infty$ for all

nondiagonal interactions, but add for the diagonal ones.

In lowest order, however [Fig. 1(a)], the terms $k_\alpha k_\beta$ will only give contributions of order m_l^2/m_W^2, which we know are small because

$$M_W > 1.8 \text{ GeV},$$

according to the CERN neutrino experiments.[3] Since the higher orders are divergent, there exists no reliable way of predicting their contribution. Stothers[4] has discussed the astrophysical evidence and concluded that the interaction for electron-type leptons is in agreement with (2)–(4), with an uncertainty in the coupling constant of one order of magnitude either way. Perkins[3] concluded on the basis of the CERN experiments that the absence of the process

$$\nu_e + e^- \rightarrow \nu_e + e^-$$

implies

$$G_{ee} \lesssim 10G$$

if G is replaced by G_{ee} in (2) for the calculation of the cross section. Since there was no significant evidence of process (a) during the CERN experiment, one can similarly conclude

$$G_{\mu\mu} < 100G.$$

We do want to stress that electrons and muons may behave differently with respect to diagonal interactions; indeed, if the muon mass has origin in the weak interactions [Fig. 1(c)], it is the only evidence of "strong" weak interaction ever seen. Since reaction (a) probably is the most promising (or only feasible) way to observe muon-type diagonal interactions, experiments to detect it should be pushed regardless of what becomes known about the corresponding electron reactions.

If some kind of an intermediate boson W exists,

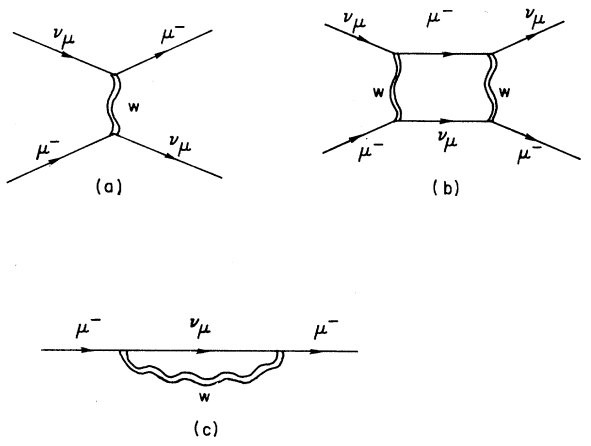

FIG. 1. Diagonal weak interactions. (a) Lowest-order neutrino-muon scattering. (b) Higher-order contribution to neutrino-muon scattering. (c) Muon mass contribution.

it can be produced via a semiweak process

$$\nu_l + Z \rightarrow Z + W^+ + l^- \tag{6a}$$

and then decay to leptons:

$$W^+ \rightarrow l^+ + \nu_l . \tag{6b}$$

Cross sections for (6a) have been given by Lee, Markstein, and Yang,[5] Bell and Veltman,[6] and others.[7] The W can also decay into other channels, and no reliable estimates for its branching ratio into leptons are known.

Since processes (1) and (6) lead to the same final state, no direct experimental separation between the two modes of production is possible (the W is very short-lived), and one has to rely on a fit to characteristic distributions in the kinematical variables of the products. We return to this question in Sec. V.

Baltay and Wachsmuth[8] have discussed an experiment to detect processes (1) in a 25-ft. neon bubble chamber, and they conclude that the background from the two-step process

$$\nu_\mu + n \rightarrow \mu^- + \pi^+ + n, \tag{7a}$$

$$\pi^+ \rightarrow \mu^+ + \nu_\mu \tag{7b}$$

is very serious, and can only be reduced to a level that makes the experiment feasible by a knowledge of the characteristic spectra.

One of the most remarkable results from the CERN neutrino experiment is that the total neutrino cross section goes as[3]

$$\sigma_{\text{tot}} = 0.6(\epsilon_1/\text{GeV}) \times 10^{-38} \text{ cm}^2,$$

where ϵ_1 is the neutrino energy. Most of the increase at high energies is due to multipion events, whereas both theory and experiment[9] indicate that the one-pion cross section levels off. CSW showed that the asymptotic cross section for reactions (1) goes as $\epsilon_1 \ln \epsilon_1$. The best chances for seeing them should therefore be in "clean" reactions with only two charged particles at the highest available energy.

Our main emphasis is therefore to calculate cross sections and spectra for (1) when the electromagnetic interaction with the nucleus is coherent. Results are also presented for reactions off single nucleons, with and without an exclusion principle correction, to allow an account of quasielastic scattering on individual nucleons. Using information from electron scattering, other inelastic excitations of the nucleus (or nucleon) could also have been included, but this was not attempted.

In Sec. II we discuss the principal methods and assumptions behind our calculation and give the formalism, in Sec. III we describe the Monte Carlo calculation, and in Sec. IV we give the results,

which are discussed in Sec. V. The square of the matrix element and details of the phase-space integration are given in Appendices A and B, respectively.

II. TOTAL CROSS SECTION AND DISTRIBUTIONS

Our main concern is to obtain distributions for the processes (1). However, rather than trying to calculate a set of differential cross sections, each in principal with a different phase-space integral, we do this by calculating a total cross section. The points in phase space where the matrix element is evaluated are picked quasirandomly to allow application of statistical methods. Each such point corresponds to a physical event, with known values of all parameters. We separate the events in histogram bins according to values of the variables in which we are interested, each "event" having a weight given by the appropriately spin-summed-squared matrix element and phase-space factors. Thus, in calculating the total cross section by scanning the phase space in a systematic way (described in Sec. III), we will at the same time collect histograms vs relevant kinematical quantities. These histograms are the same quantities which one would observe in an experiment.

The two diagrams which we will take into account are shown in Fig. 2. Because we only consider one-photon exchange, the hadronic and leptonic parts will factor out and, in much the same fashion as CSW, we can write the total cross section

$$\sigma = \frac{2Z^2\alpha^2G^2}{(2\pi)^6 4M\epsilon_1}\int \frac{d^3P'}{2E'}\frac{d^3p_3}{2\epsilon_3}\frac{d^3p_4}{2\epsilon_4}\frac{d^3p_2}{2\epsilon_2} \times \delta^4(P+p_1-P'-p_2-p_3-p_4)H_{\alpha\beta}L_{\alpha\beta}\frac{1}{(q^2)^2}. \quad (8)$$

The notation for the momenta is indicated in Fig. 2; M is then the target mass, E' is the final target energy, and ϵ_1–ϵ_4 are the lepton energies;

$$q = P - P', \quad q^2 = q\cdot q = q_\mu q_\mu ,$$

and $L_{\alpha\beta}$ is the square of the lepton current summed over spins:

$$L_{\alpha\beta} = \mathrm{Tr}[\gamma_\lambda(1+\gamma_5)\not p_1\gamma_\sigma(1+\gamma_5)\not p_2]\mathrm{Tr}\{[\gamma_\alpha(i\not p_4 - i\not q + m_4)^{-1}\gamma_\lambda(1+\gamma_5)+\gamma_\lambda(1+\gamma_5)(i\not q - i\not p_3 + m_3)^{-1}\gamma_\alpha] \times(-m_3 - i\not p_3)[\gamma_\beta(i\not q - i\not p_3 + m_3)^{-1}\gamma_\sigma(1+\gamma_5)+\gamma_\sigma(1+\gamma_5)(i\not p_4 - i\not q + m_4)^{-1}\gamma_\beta](m_4 - i\not p_4)\}, \quad (9)$$

where we followed CSW and made a Fierz transformation.[10] Also, m_3 and m_4 are the outgoing lepton masses, and $H_{\alpha\beta}$ is the square of the matrix element of the hadronic electromagnetic current. For single-nucleon states we have

$$\langle P'|J_\alpha^{\mathrm{em}}|P\rangle = \bar U(P')\left[i\gamma_\alpha F_1(q^2) + \frac{F_2(q^2)}{2M}i\sigma_{\alpha\beta}q_\beta\right]U(P),$$

where u are the Dirac spinors and F_1, F_2 are the usual form factors. Summing over final spin and averaging over initial spin gives

$$H_{\alpha\beta} = \frac{G_E^{\,2} - G_M^{\,2}}{1+x}(P+P')_\alpha(P+P')_\beta + G_M^{\,2}(q^2\delta_{\alpha\beta} + 2P_\alpha P'_\beta + 2P_\beta P'_\alpha), \quad (10)$$

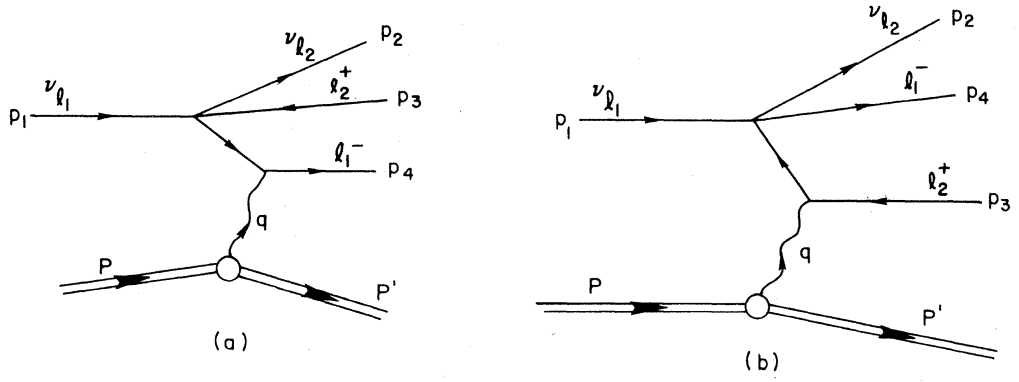

FIG. 2. Diagrams for trilepton production by the point four-fermion interaction.

where

$$x = q^2/4M^2,$$
$$G_M = F_1 + F_2 = \mu_T G,$$
$$\mu_T = \begin{cases} 2.792 & \text{for protons} \\ -1.913 & \text{for neutrons} \end{cases} \qquad (11)$$
$$G_E = F_1 - xF_2 = zG,$$
$$z = \begin{cases} 1 & \text{for protons} \\ 0 & \text{for neutrons} \end{cases}$$
$$G = (1 + 4.88x)^{-2}.$$

The dipole fit for the form factors adopted[11] agrees well enough with the data for our purpose. For coherent scattering from a spin-zero nucleus, one has

$$H_{\alpha\beta} = F^2(q^2)(P+P')_\alpha (P+P')_\beta, \qquad (12)$$

which agrees with the Coulomb part of the one-nucleon tensor when all spin corrections are omitted. We will assume that the nuclear form factor is given as a Fourier transform of the charge distribution evaluated in the Breit frame ($q_0 = 0$):

$$F(q^2) = \int \rho(r) e^{i\vec{q}\cdot\vec{r}} d^3r \Big/ \int \rho(r) d^3r. \qquad (13)$$

We are at this stage only interested in a description of the average A behavior for nuclei, and will assume a two-parameter Fermi distribution for the charge density,

$$\rho(r) = \rho_F(r) = [1 + e^{(r-c)/t}]^{-1}, \qquad (14)$$

and denote the corresponding form factor (13) by F_F. We evaluated F_F by means of a numerical Gaussian integration. Data from electron scattering[12] indicate that

$$c = (1.18A^{1/3} - 0.48)\ \text{F}, \qquad (15)$$
$$t = 0.55\ \text{F} \quad (A > 8).$$

In Fig. 3, F_F is compared with the experimental data of Sick and McCarthy,[13] together with the two other form factors

$$F_{\text{I}} = (1 + a^2q^2/12)^{-2}, \qquad (16)$$
$$F_{\text{II}} = e^{-a^2q^2/6},$$

where a, the root-mean-square radius of the charge distribution, is given approximately by[12]

$$a = (0.58 + 0.82A^{1/3})\ \text{F}. \qquad (17)$$

With this choice of a, the quantities F_F, F_{I}, and F_{II} have all approximately the same expansion to first order in q^2, for all values of A. F_{I} and F_{II} are equivalent to the form factors used by CSW with

$$a = 0.93A^{1/3}\ \text{F}.$$

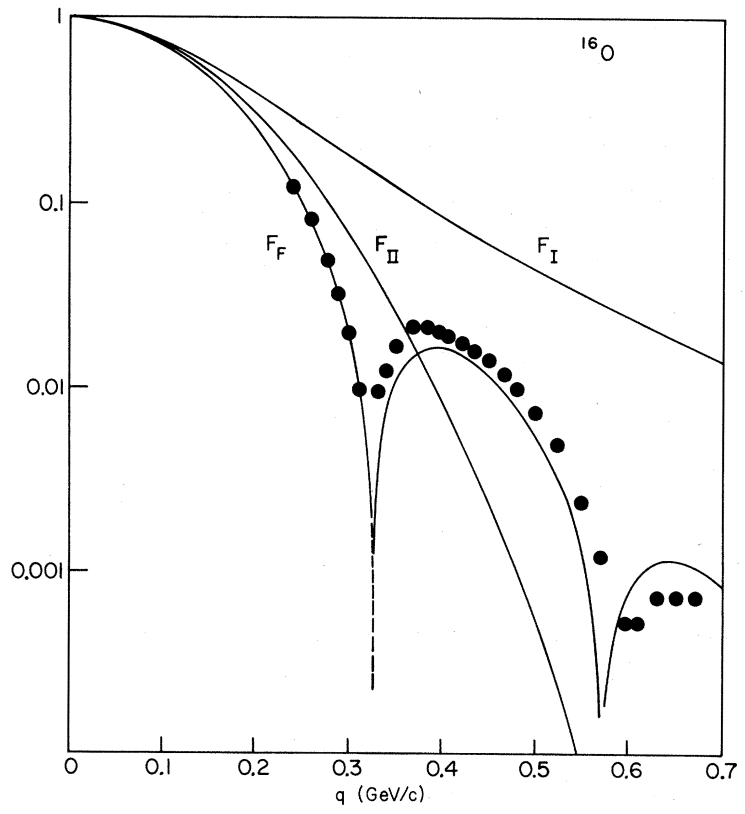

FIG. 3. Comparison of form factors for ^{16}O. F_{I} and F_{II} are given by Eq. (16), with Eq. (17). F_F is given by (13) with (14) and (15). The filled circular points are experimental data of Ref. 3.

Evidently, the phenomenological form factor F_F based on the Fermi charge distribution gives an excellent fit through the first (forward) diffraction maximum, which turns out to be overwhelmingly the most important region in our case, making the slight miss on the second maximum insignificant for our purposes. We return to this question in Sec. IV.

Gauge invariance of the electromagnetic current means

$$q_\alpha L_{\alpha\beta} = q_\beta L_{\alpha\beta} = q_\alpha H_{\alpha\beta} = q_\beta H_{\alpha\beta} = 0 .$$

Since $P' = P - q$, the effective part of $H_{\alpha\beta}$ can be written as

$$H_{\alpha\beta}^{\text{eff}} = 4P_\alpha P_\beta F^2(q^2) \tag{18a}$$

for coherent reactions on a spin-zero nucleus and

$$H_{\alpha\beta}^{\text{eff}} = 4P_\alpha P_\beta (G_E{}^2 + xG_M{}^2)/(1+x) + \delta_{\alpha\beta} q^2 G_M{}^2 \tag{18b}$$

for single nucleons. We therefore only need to know the contractions $P\cdot L\cdot P$ and $\delta_{\alpha\beta}L_{\alpha\beta}$. To evaluate the traces, extensive use was made of the tricks given by Chisholm,[14] in particular, all γ_5's can be eliminated by contracting the product of traces to one trace.

The result of the trace calculation is given in Appendix A, the phase-space integration is discussed in Appendix B, where we also give expressions for the invariants in terms of the integration variables.

Calculation of the coherent reaction (1), for any spin-zero nuclear target, using (18a), gives a result independent of any nuclear model, since the form factor F is experimentally measured by electron scattering. Nuclear excitations may be taken into account only in a model-dependent fashion. If quasielastic excitations are included, the cross section for scattering off a nucleus with Z protons and N neutrons can approximately be written as

$$d\sigma_{\text{tot}} = d\sigma_{\text{coh}} + X(|\vec{q}|)[N\, d\sigma_n + Z d\sigma_p] , \tag{19}$$

where X is an exclusion-principle factor and $d\sigma_{n,p}$ is a partial cross section for a free neutron (proton) target. For the numerical evaluations we have used

$$X(|\vec{q}|) = \begin{cases} 1.5(|\vec{q}|/2p_f) - 0.5(|\vec{q}|/2p_f)^3 , & |\vec{q}| < 2p_f \\ 1, & |\vec{q}| > 2p_f \end{cases} \tag{20}$$

$$p_f = 235 \text{ MeV}/c$$

which is correct for an ideal Fermi gas having the same density as that of protons (or neutrons) in the nucleus.[15] This model is known to work fairly well for electron scattering.[16]

III. MONTE CARLO CALCULATION

After eliminating the δ function and a trivial azimuthal integration, the total cross section will be proportional to a seven-dimensional integral of the type

$$I = \int_{\underline{u}_1}^{\bar{u}_1} du_1 \cdots \int_{\underline{u}_7}^{\bar{u}_7} du_7 (q^2)^{-2} L_{\alpha\beta} H_{\alpha\beta} J(u) , \tag{21}$$

where u_i $(i = 1, \ldots, 7)$ are the integration variables, the choice of which we discuss below, and $\bar{u}_i$ and $\underline{u}_i$ their upper and lower limits, respectively. $\underline{u}_k$ and $\bar{u}_k$ are in general functions of $u_1, \ldots, u_{k-1}$. J contains the Jacobian factor of the transformation from $d^3p_2 d^3p_3 d^3p_4 d^3P' \delta^4(P + p_1 - P' - p_2 - p_3 - p_4)$ to $du_1 \cdots du_7$.

We follow the same method as CSW and divide the ith integration range into N_i equal parts. Thus the phase space is divided into

$$N = \prod_{i=1}^{7} N_i$$

elements. Within each element two points are picked at random. A statistically unbiased estimate for the integral is then

$$I = \frac{1}{2N} \sum_{n_1=1}^{N_1} \cdots \sum_{n_7=1}^{N_7} [f(\{u\}_1) + f(\{u\}_2)] ,$$
$$f(\{u\}) = (q^2)^{-2} (L_{\alpha\beta} H_{\alpha\beta}) J(\{u\}) \prod_{i=1}^{7} (\bar{u}_i - \underline{u}_i) . \tag{22}$$

An unbiased estimator of the corresponding variance is

$$\sigma^2 = \frac{1}{4N^2} \sum_{n_1=1}^{N_1} \cdots \sum_{n_7=1}^{N_7} [f(\{u\}_1) - f(\{u\}_2)]^2 . \tag{23}$$

To keep the variance small, which means an efficient evaluation of I, the variables u_1–u_7 should be chosen such that the corresponding Jacobian makes $f(\{u\})$ vary as little as possible through the integration region.

For reactions (a) and (b), we have used

$$u_1 = \int_{q^2}^{\infty} F^2(x) dx ,$$
$$u_2 = -(p_2 + p_3 + p_4)^2 - (m_3 + m_4)^2 ,$$
$$u_3 = \ln(q^2 - 2p_3 \cdot q) \equiv \ln D_3 ,$$
$$u_4 = [-(p_2 + p_4)^2 - m_4{}^2]^2 \equiv (W_c{}^2 - m_4{}^2)^2 , \tag{24}$$
$$u_5 = \varphi_3 ,$$
$$u_6 = \ln(q^2 - 2p_4 \cdot q) \equiv \ln D_4 ,$$
$$u_7 = \varphi_4 .$$

The Jacobian factor corresponding to u_1 eliminates the form-factor dependence in (22). For reactions on single nucleons, $F(q^2)$ was, of course, replaced by $G(q^2)$. For $F = F_F$ [Eqs. (13–15)], the problem of inversion was solved by creating a catalog which gives the value of q^2 corresponding to a particular value of u_1. This catalog must of course be large enough that no systematic errors are

TABLE I. Total cross section and average values of kinematical quantities for processes (a)–(c), Eq. (1).

ϵ_1 (GeV)	Nucleus	σ_T/Z^2 (10^{-44} cm^2)	T_2 [a] (GeV)	T_3 [a] (GeV)	T_4 [a] (GeV)	Δp_{113} (MeV/c)	Δp_{114} (MeV/c)	p_{t3} (MeV/c)	p_{t4} (MeV/c)	q^2 (GeV/c)^2	W_{34}^2 (GeV^2)
					Coherent reaction (a) $\nu_\mu + Z \to \nu_\mu + Z + \mu^+ + \mu^-$						
1.5	Pb	0.00883	0.394	0.378	0.516	7.29	6.84	67.5	74.8	0.00631	0.0738
4.0	Pb	0.180	1.39	0.947	1.45	6.70	6.26	93.7	110	0.00421	0.104
8	Pb	0.877	3.13	1.73	2.93	6.46	6.00	118	146	0.00348	0.143
15	Pb	2.94	6.38	2.94	5.47	6.26	5.80	146	189	0.00307	0.202
40	Pb	15.2	18.4	6.73	14.7	5.90	5.51	204	287	0.00269	0.383
1.5	Fe	0.300	0.433	0.348	0.508	10.5	9.91	78.6	89.2	0.0102	0.0831
4.0	Fe	0.431	1.47	0.872	1.44	9.89	9.19	108	131	0.00769	0.124
8	Fe	1.83	3.27	1.60	2.92	9.44	8.75	136	173	0.00665	0.177
15	Fe	5.48	6.57	2.74	5.48	9.12	8.44	168	225	0.00604	0.259
40	Fe	27.0	18.9	6.34	14.6	8.62	8.01	235	341	0.00536	0.509
1.5	C	0.0768	0.462	0.320	0.506	16.0	14.7	92.3	107	0.0182	0.0963
4.0	C	0.877	1.53	0.817	1.44	14.7	13.4	126	156	0.0146	0.152
8	C	3.43	3.37	1.51	2.91	13.9	12.7	157	206	0.0130	0.224
15	C	10.1	6.72	2.59	5.48	13.4	12.2	194	265	0.0120	0.338
40	C	45.2	19.2	6.08	14.5	12.8	11.6	275	405	0.0110	0.691
					Incoherent reaction (a) $\nu_\mu + N \to \nu_\mu + N + \mu^+ + \mu^-$ [b]						
1.5	p	0.488	0.477	0.280	0.477	44.2	38.8	144	166	0.102	0.143
4	p	4.93	1.57	0.731	1.42	46.0	39.1	208	258	0.125	0.300
15	p	51.0	6.82	2.41	5.48	45.2	38.4	338	458	0.144	0.856
1.5	p [c]	0.346	0.479	0.270	0.470	52.6	46.2	158	183	0.130	0.156
4	p [c]	3.46	1.56	0.715	1.42	56.2	47.4	234	289	0.165	0.346
15	p [c]	3.54	6.84	2.38	5.47	56.3	47.7	386	523	0.196	1.04
1.5	n	0.0605	0.509	0.273	0.422	64.0	57.9	177	194	0.161	0.168
4	n	0.610	1.61	0.729	1.33	72.4	62.0	274	321	0.223	0.405
15	n	6.32	6.85	2.40	5.39	75.2	64.3	462	608	0.284	1.32
1.5	n [c]	0.504	0.505	0.270	0.416	69.8	63.9	186	205	0.184	0.176
4	n [c]	0.529	1.60	0.731	1.32	77.9	66.7	287	334	0.249	0.428
15	n [c]	5.61	6.82	2.42	5.38	79.9	68.2	480	629	0.313	1.40
					Coherent reaction (b) $\nu_\mu + Z \to \nu_e + Z + e^+ + \mu^-$						
1.5	Pb	0.198	0.498	0.124	0.782	8.89	4.78	33.1	71.4	0.00273	0.0310
4.0	Pb	1.46	1.56	0.304	2.03	7.29	4.86	42.4	108	0.00223	0.0495
8	Pb	4.71	3.36	0.576	3.96	6.55	4.81	52.2	145	0.00202	0.0748
15	Pb	12.2	6.60	1.04	7.25	6.01	4.71	64.8	187	0.00190	0.114
40	Pb	46.6	18.7	2.66	18.5	5.45	4.64	92.9	287	0.00178	0.243
1.5	Fe	0.349	0.519	0.142	0.733	12.5	7.17	42.8	84.2	0.00511	0.0380
4.0	Fe	2.35	1.59	0.342	1.96	10.4	7.09	54.9	127	0.00436	0.0641
8	Fe	7.28	3.43	0.639	3.83	9.35	7.01	67.8	169	0.00404	0.0997
15	Fe	18.4	6.71	1.14	7.04	8.66	6.84	83.4	219	0.00386	0.157
40	Fe	68.9	19.0	2.87	18.1	8.01	6.74	121	338	0.00368	0.346
1.5	C	0.550	0.530	0.159	0.704	17.1	10.6	54.3	99.1	0.00941	0.0468
4.0	C	3.49	1.63	0.376	1.89	14.6	10.3	70.0	147	0.00852	0.0833
8	C	10.6	3.49	0.704	3.70	13.2	10.1	86.4	197	0.00806	0.134
15	C	26.0	6.84	1.26	6.79	12.6	9.98	108	259	0.00798	0.220
40	C	97.5	19.1	3.20	17.6	11.5	9.60	156	390	0.00760	0.482

TABLE I *(Continued)*

ϵ_1 (GeV)	Nucleus	σ_T/Z^2 (10^{-44} cm^2)	T_2 [a] (GeV)	T_3 [a] (GeV)	T_4 [a] (GeV)	Δp_{113} (MeV/c)	Δp_{114} (MeV/c)	p_{t3} (MeV/c)	p_{t4} (MeV/c)	q^2 (GeV/c)^2	W_{34}^2 (GeV^2)
					Incoherent reaction (b) $\nu_\mu + N \to \nu_e + N + e^+ + \mu^-$ [b]						
1.5	p	1.40	0.527	0.214	0.623	36.9	26.8	98.7	145	0.0566	0.0810
4	p	9.51	1.62	0.523	1.71	38.4	29.1	146	228	0.0790	0.192
15	p	79.0	6.82	1.73	6.29	38.0	30.7	244	414	0.102	0.629
1.5	p [c]	0.722	0.523	0.243	6.58	51.5	38.4	129	175	0.0928	0.106
4	p [c]	5.18	1.62	0.606	1.70	54.1	41.6	194	278	0.130	0.263
15	p [c]	44.4	6.89	1.99	5.94	54.4	44.4	327	518	0.169	0.879
1.5	n	0.0853	0.542	0.302	0.474	65.6	55.3	16.5	196	0.141	0.124
4	n	0.725	1.65	0.729	1.41	72.5	59.8	256	320	0.205	0.337
15	n	6.87	6.91	2.30	5.54	75.0	62.9	436	610	0.272	1.19
1.5	n [c]	0.0670	0.534	0.311	0.459	73.1	62.4	178	209	0.169	0.135
4	n [c]	0.608	1.63	0.749	1.39	79.3	65.5	274	336	0.236	0.365
15	n [c]	5.97	6.89	2.35	5.49	80.6	67.5	460	635	0.305	1.28
					Coherent reaction (c) $\nu_e + Z \to \nu_e + Z + e^+ + e^-$						
1.5	Pb	1.13	0.736	0.195	0.568	5.38	4.39	30.3	46.5	0.00124	0.00823
4	Pb	4.20	2.02	0.479	1.50	5.25	4.39	44.1	73.2	0.00134	0.0203
15	Pb	20.9	7.78	1.56	5.66	5.31	4.47	76.2	140	0.00149	0.0733
1.5	Fe	1.48	0.720	0.207	0.571	7.57	6.23	37.1	55.9	0.00247	0.0118
4	Fe	5.56	1.98	0.493	1.53	7.66	6.31	54.8	88.4	0.00279	0.0304
15	Fe	29.2	7.69	1.67	5.65	7.54	6.42	94.8	167	0.00308	0.105
1.5	C	1.82	0.716	0.215	0.568	11.0	8.74	47.5	67.0	0.00493	0.0174
4	C	7.30	1.96	0.499	1.54	10.8	8.80	66.2	106	0.00555	0.0439
15	C	37.9	7.69	1.78	5.53	11.1	9.40	121	205	0.00641	0.159

[a] Subscripts 2, 3, and 4 refer to the three outgoing leptons as indicated in Fig. 2.

[b] These results may be used to account for incoherent reactions in a nuclear target (Z,N). One weights the proton results by Z, the neutron results by N (the coherent results by Z^2). The exclusion-principle corrected[c] results should be used for this.

[c] An exclusion-principle correction factor (20) has been applied inside all phase-space integrations.

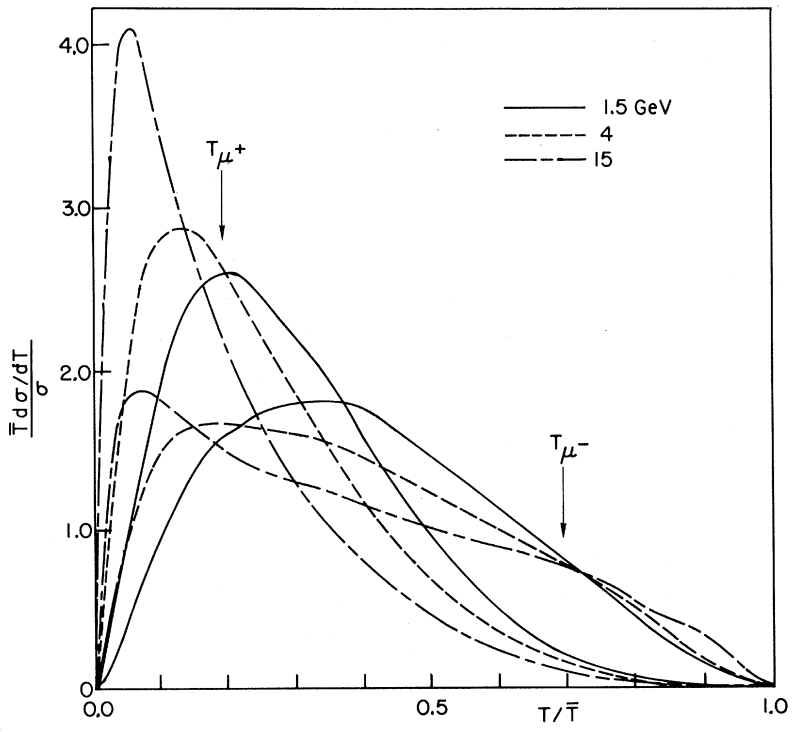

FIG. 4. Distributions in charged-lepton kinetic energy from the coherent process (a), for a ^{208}Pb target and three values of neutrino beam energy ϵ_1. (These curves, as are all of Figs. 4–16, are actually smooth-drawn envelopes of histograms having about 100 bins. The shapes of the curves within 1–2% of the endpoints are therefore necessarily conjectural.)

introduced, but this causes no problem.

The form factor is indeed the dominating factor in this integration, and cuts off the integration in q^2 at such a low value that the photon propagator is approximately canceled by factors from phase space and the matrix element, and needs therefore no extra treatment to reduce variance.

The variables u_3 and u_6 were found to be very effective for the two-muon case. They completely eliminate the lepton propagators, which appear in the cross terms of the squared matrix element, and apparently also effectively cancel the propagator dependence in the direct terms.

However, for the two-electron case,

$$u_3 = D_3\,, \qquad u_6 = D_4\,, \tag{25}$$

was found more efficient, because in the region $D_i \ll q^2$ which is large in logarithmic scale for the 2-e case, the propagator effect is canceled by phase space. With the choice (24) for variables, the total cross section can be written

$$\sigma = \frac{G^2\alpha^2 Z^2}{2(2\pi)^6 M\epsilon_1} I\,, \tag{26}$$

where I is defined in (22), and the Jacobian is

$$J = \left[\frac{2\pi}{8E_1 MF^2(q^2)}\right]\left[\frac{D_3}{16(-q\cdot p_1)u_4^{1/2}}\right]\left[\frac{D_4}{8|\vec{q}|^c W_c}\right], \tag{27}$$

the successive square brackets stemming from the d^3P', d^3p_3, and $d^3p_4 d^3p_2\delta^4(\cdots)$ integrations in (8). The phase-space integral is worked out in detail in Appendix B, where also the limits are given.

For a given neutrino energy and nucleus, a computer run to produce eight single distributions and five double distributions with a statistical standard deviation in the total cross section of about 1% took less than one minute on the Stanford IBM 360/67, which is much faster than we dared to hope for when we started this calculation.

IV. RESULTS

We calculated distributions for the following quantities:

$$\left.\begin{aligned} &T_i\,,\\ &p_{ti} \equiv 2|\vec{p}_i|\sin\tfrac{1}{2}\theta_i\,,\\ &\Delta p_{\parallel i} \equiv |\vec{p}_i|(1-\cos\theta_i)\,, \end{aligned}\right\} \; i = 3,4\ (\equiv l^+, l^-)$$
$$W_{34}{}^2 \equiv -(p_3+p_4)^2\,, \qquad q^2\,, \qquad T_2\,, \tag{28}$$

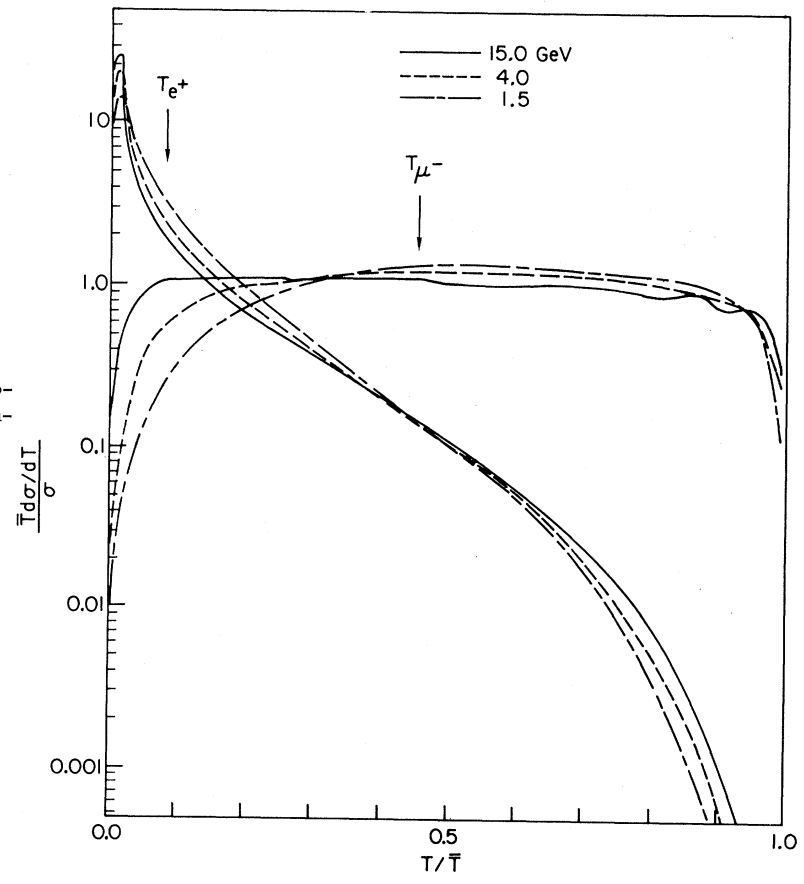

FIG. 5. Distributions in charged-lepton kinetic energy, T_{μ^+} and T_{μ^-}, from the coherent process (b), plotted with a logarithmic ordinate scale. The target is ^{208}Pb; the energies labeling the curves are ϵ_1.

where T_i are the lepton laboratory kinetic energies, $|\vec{p}_i|$ are the momenta, and θ_i is the angle in the lab frame with respect to the incoming neutrino.

For small angles, $p_{ti} \approx p_i \theta_i$ thus nearly coinciding with the usual definition of transverse momentum $p_{\perp i}$.

The average values of these quantities together with the total cross sections for processes a, b, and c are given in Table I for proton (with and without an exclusion principle factor), neutron, and three nuclei: ^{12}C, ^{56}Fe, and ^{208}Pb. The exclusion-principle-corrected neutron and proton results, weighted by N and Z, respectively, may be used to correct the coherent results (for nuclear targets) for incoherent reactions off single nucleons; one uses the prescription (19). The neutrino energies (three or five values) are chosen to be relevant for the spectra at CERN, Serpukhov, and NAL. The total cross section is given in units of

$$\sigma_0 = Z^2 10^{-44} \text{ cm}^2 .$$

The values given in Table I have statistical error (standard deviation) of about 1% or less. For interpolation to find the total cross section for an A intermediate to those given, the formula

$$\sigma/\sigma_0 = c_1/a^2 + c_2 \tag{29}$$

can be used where a is the rms radius (17) and c_1 and c_2 are the constants to be fitted to the two adjacent nuclei. The first term on the right-hand side follows from the cutoff in the form factor. c_2 is a small correction to take into account variations in the matrix element apart from the form-factor dependence.

The distributions in kinetic energy of the charged leptons produced off ^{208}Pb at three different neutrino energies (1.5, 4.0, and 15.0 GeV) are given in Figs. 4 and 5 for processes (a) and (b), respectively. (Figure 5 has the ordinate plotted logarithmically.) The same distributions are graphed in Fig. 6 for process (a) occurring at the one energy

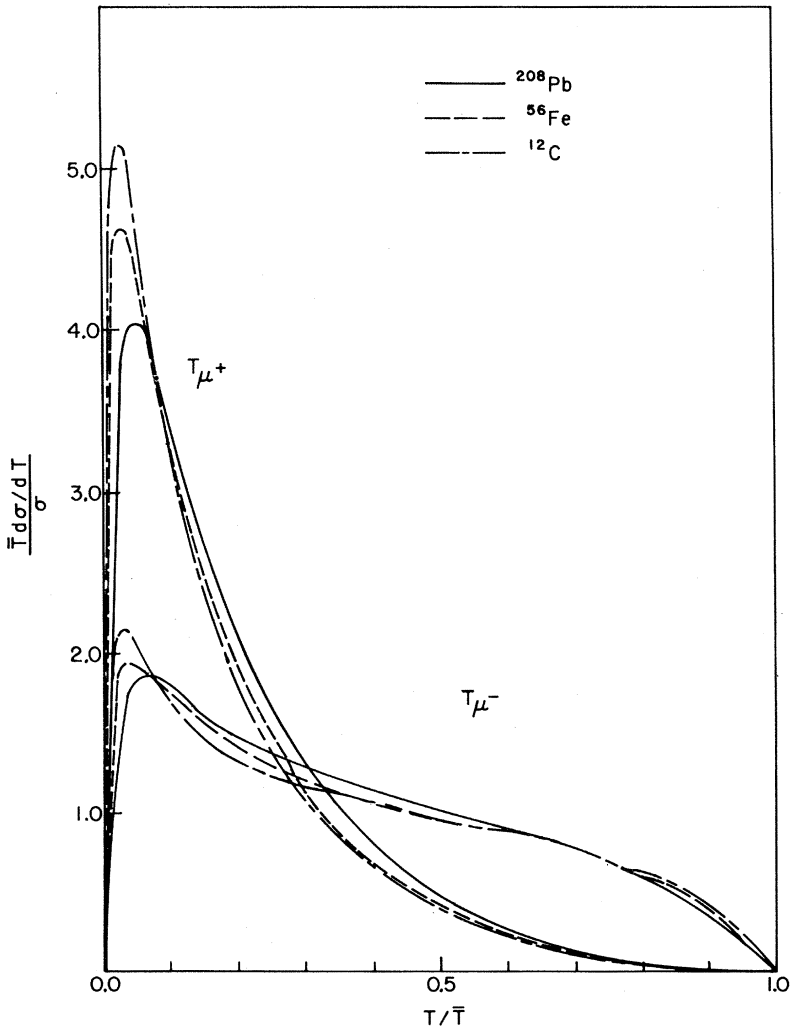

FIG. 6. Distributions in charged lepton kinetic energy T_{μ^+} and T_{μ^-}, from the coherent process (a). The neutrino beam energy is 15 GeV.

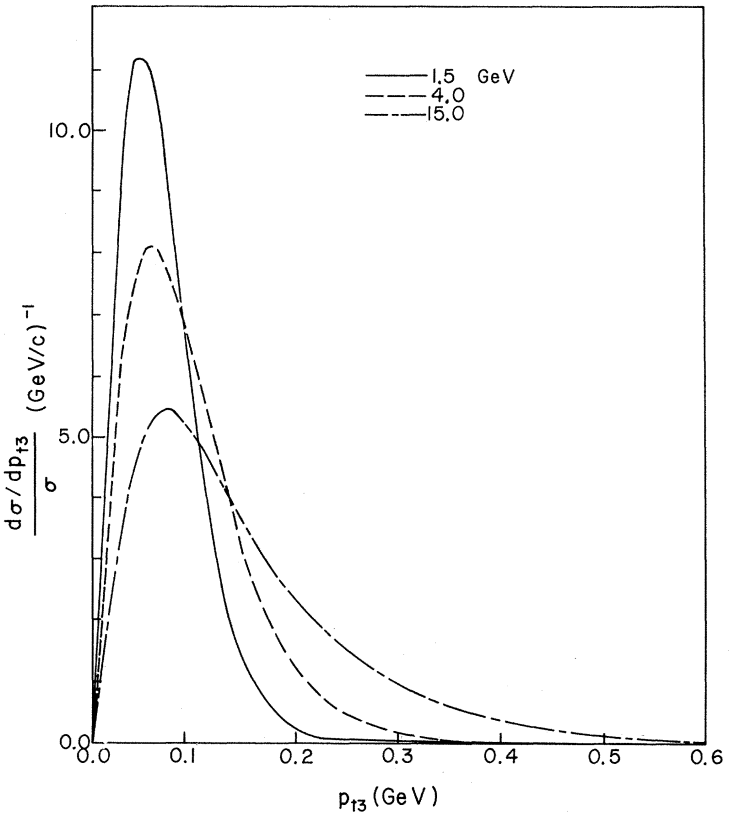

FIG. 7. Distributions in transverse momentum p_{t3} of the μ^+ from coherent reaction (a), off ^{208}Pb.

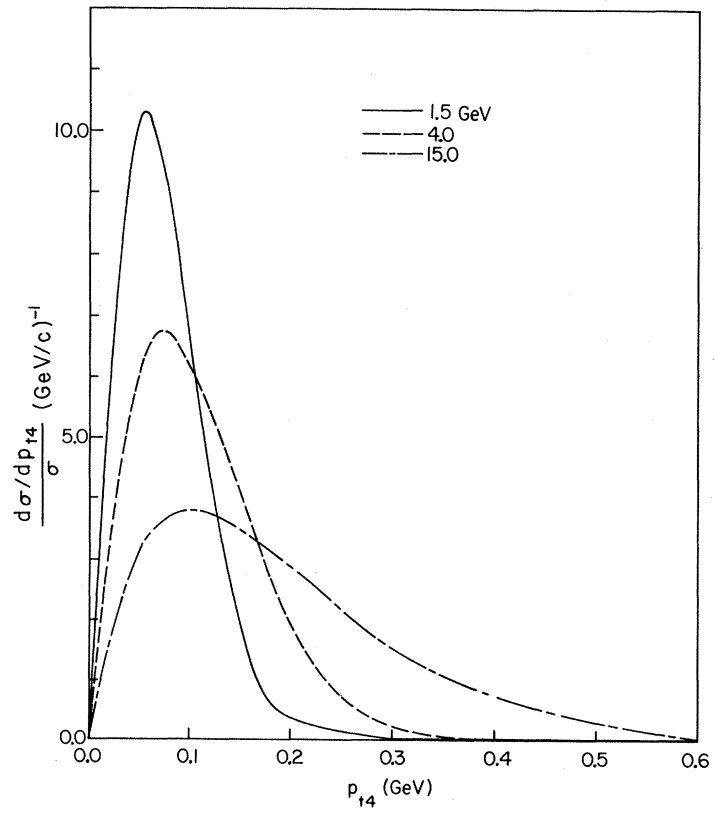

FIG. 8. Distributions in transverse momentum p_{t4} of the μ^- from coherent reaction (a), off ^{208}Pb.

15 GeV on the three target nuclei ^{12}C, ^{56}Fe, and ^{208}Pb. The abscissa in all these cases is the laboratory-frame kinetic energy, in units of its maximum, $T_i/\overline{T}_i$:

$$\overline{T}_i = \tfrac{1}{2}W_A^{-2}\{(M+\epsilon_1)[W_A^2 + m_i^2 - (M+m_j)^2] + \epsilon_1\{[W_A^2 + m_i^2 - (M+m_j)^2]^2 - 4W_A^2 m_i^2\}^{1/2}\} - m_i , \tag{30}$$

where $i=3$, $j=4$ for the energy of the positive lepton, and $i=4$, $j=3$ for the energy of the negative one. Furthermore, W_A, defined by

$$W_A^2 = M^2 + 2M\epsilon_1 ,$$

is the available energy squared in the center-of-mass system. The enormous difference between the positive and negative leptons is the most notable feature of Fig. 4 and 5. The positive lepton tends to be slow, and the negative one fast (see also Table I). The relative lack of target dependence in Fig. 6 is also striking. In these graphs, as indeed in all to follow, the curves are normalized to unit area.

Figures 7–14 depict distributions in the variables $p_{ti}(i=3,4)$. Figures 7 and 8, dealing with p_{t3} and p_{t4}, respectively, compare the distributions occurring for process (a) at the standard three incoming neutrino energies on ^{208}Pb. Figures 9 and 10 do the same for process (b). Figures 11 and 12 compare process (a) at 15 GeV among three targets, for p_{t3} and p_{t4}, respectively. Figures 13 and 14 compare distributions in p_{t3} and p_{t4}, respectively, from process (a) with protons as a target; the solid curves represent free protons, but the dashed curves result when the exclusion-principle correction (20) is applied. The exclusion-principle correction apparently has little effect on these distributions beyond shifting them outward very slightly.

Figure 15 displays a logarithmic plot of the distributions in $\Delta p_{\parallel 3}$ and $\Delta p_{\parallel 4}$ occurring for process (a) at 15 GeV, comparing the three standard nuclear targets. There is very little difference between the positive and negative leptons with respect to this graph. Although not displayed, the dependence on incoming neutrino energy of these distributions is extremely slight over the range of energies studied (1.5 to 40 GeV); this may be confirmed by referring to columns 7 and 8 of Table I. This makes these distributions very useful since they may easily be applied without change to the typical experimental case of a broad incoming neutrino spectrum.

Figure 16 shows the distribution in W_{34}^2 from process (a) off ^{208}Pb, comparing the three energies;

$$W_{34}^2 \equiv -(p_3+p_4)^2 = 2|\vec{p}_3||\vec{p}_4|(1-\cos\psi_{34}) + O(m_3^2, m_4^2) ,$$

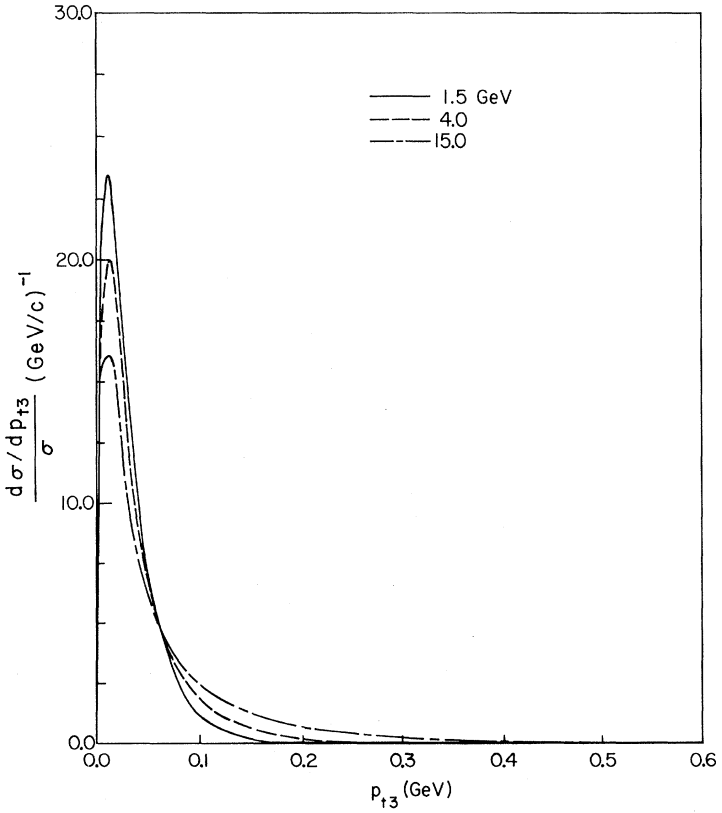

FIG. 9. Distributions in transverse momentum p_{t3} of the e^+ from coherent reaction (b), off ^{208}Pb.

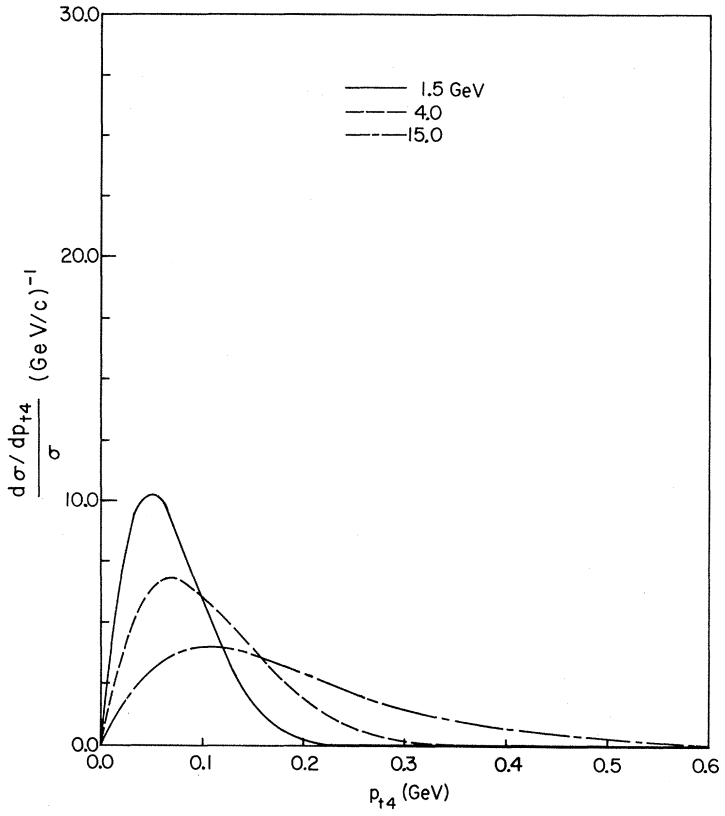

FIG. 10. Distributions in transverse momentum p_{t4} of the μ^- from coherent reaction (b), off ^{208}Pb.

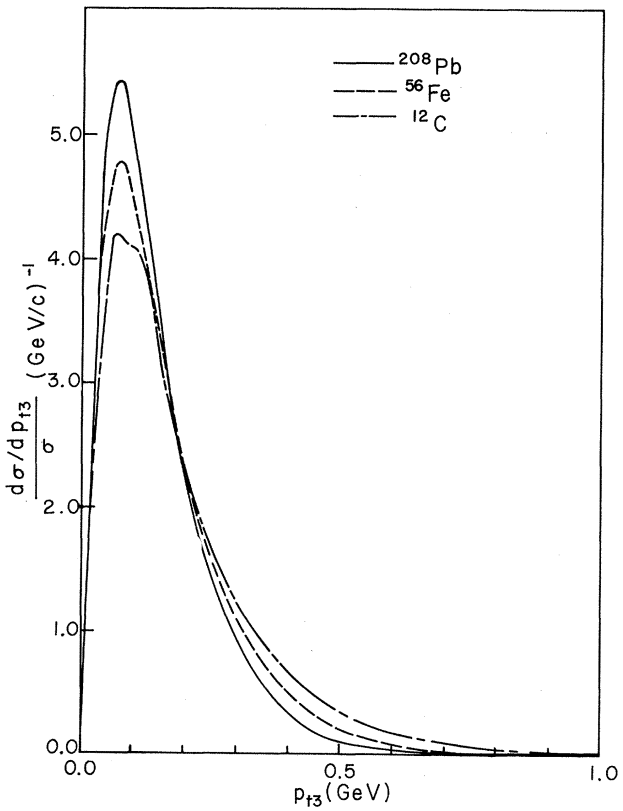

FIG. 11. Distributions in transverse momentum p_{t3} of the μ^+ from coherent reaction (a), at $\epsilon_1 = 15$ GeV.

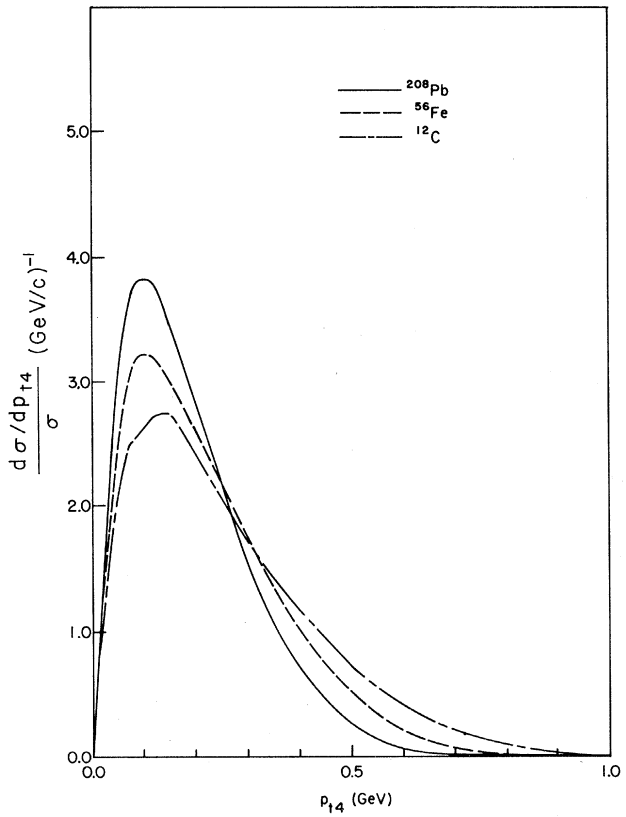

FIG. 12. Distributions in transverse momentum p_{t4} of the μ^- from coherent reaction (a), at $\epsilon_1 = 15$ GeV.

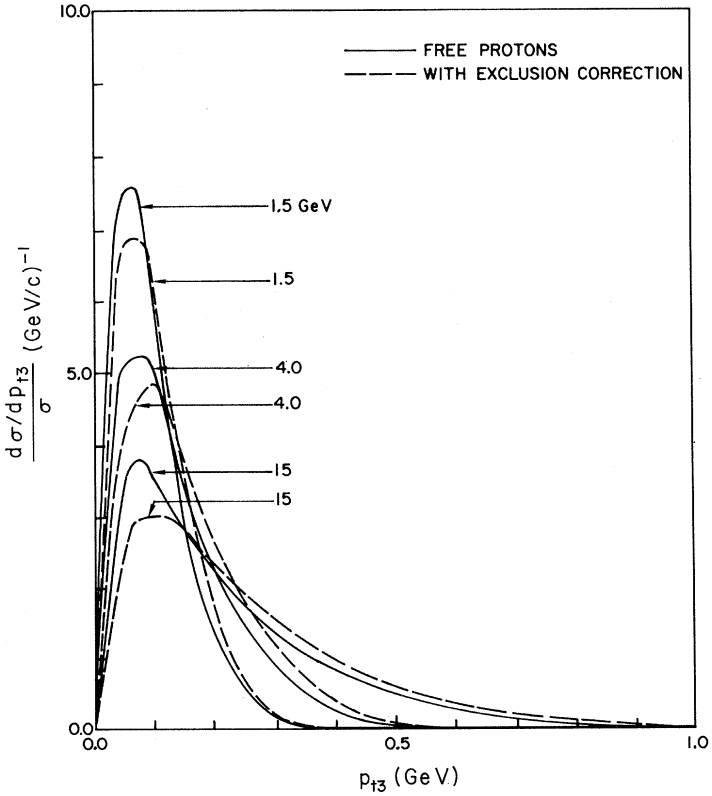

FIG. 13. Distributions in transverse momentum p_{t3} of the μ^+ from incoherent process (a). The solid curve is the free-proton result. The dashed curve is the result for protons in a Fermi gas with Fermi momentum 235 MeV/c.

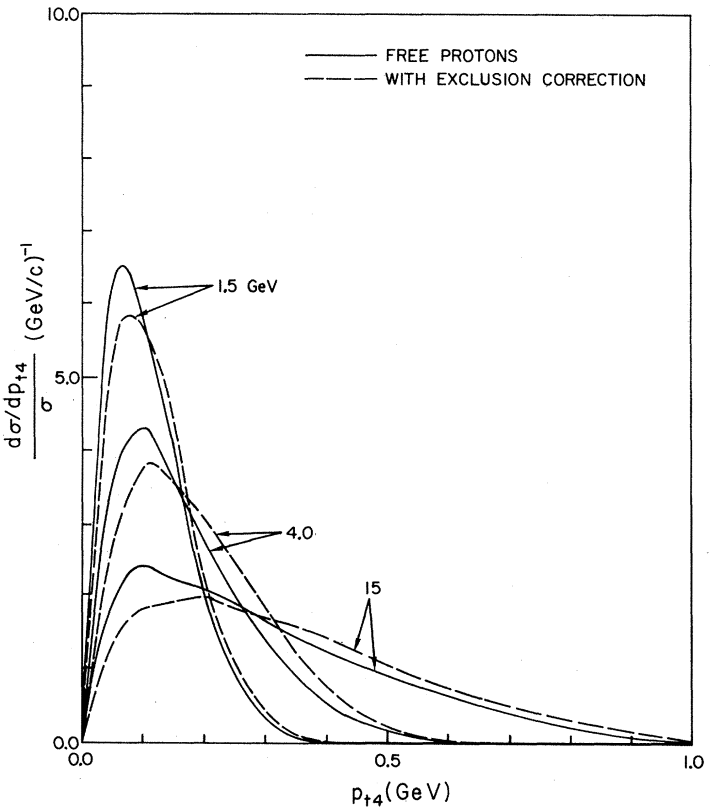

FIG. 14. Distributions in transverse momentum p_{t4} of the μ^- from incoherent process (a). Compare Fig. 13.

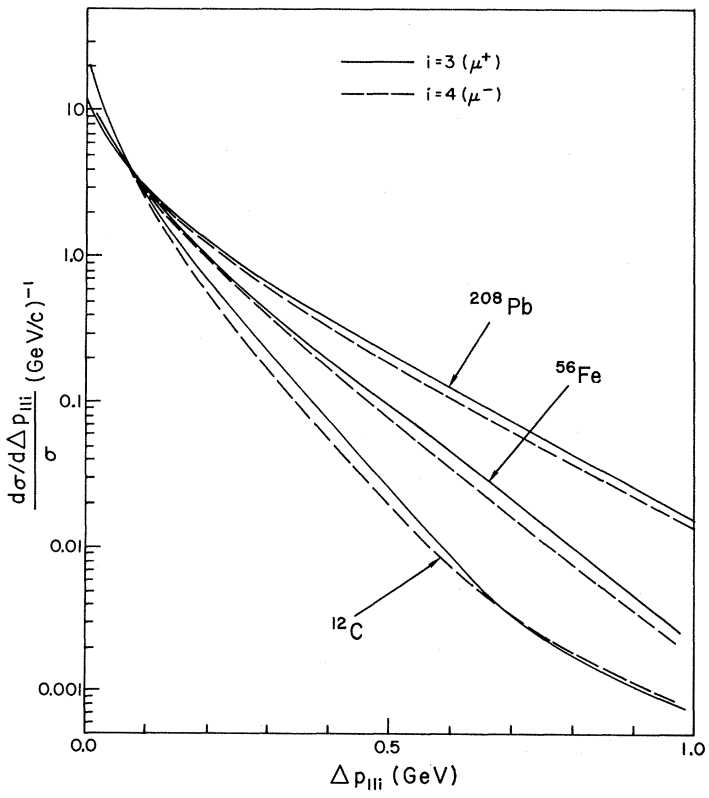

FIG. 15. Distributions in Δp_{113} and Δp_{114} (3 = μ^+, 4 = μ^-) of charged leptons from coherent process (a) at $\epsilon_1 = 15$ GeV.

where ψ_{34} is the angle in the lab frame between $\vec{p}_3$ and $\vec{p}_4$.

Figures 17 and 18 display the histograms of double distributions in T_i and p_{ti} ($i=3$ for Fig. 17, $i=4$ for Fig. 18) from process (a) off ^{208}Pb at $\epsilon_1 = 15$ GeV. In each figure ten histograms are plotted, with successively shifted origins, and histogram k pertains to kinetic energies from $(k-1)/10$ of the maximum to $k/10$ of the maximum. Each of the ten histograms contains fifteen bins, and the nth bin contains transverse momenta from $(n-1)\times 0.05$ GeV/c to $n\times 0.05$ GeV/c. The height of a given bin in a given histogram is proportional to the fraction of the total cross section which consists of events having T_i and p_{ti} within the specified limits for that bin and histogram.

V. DISCUSSION

To test our programs, we used the same form factors as CSW and we then reproduced their results to within 1% accuracy for several energies. We consider this to be a critical check on our calculation of the matrix element and the phase-space integrations. We made a further check by inverting the order of the phase-space integrations d^3p_3 and d^3p_4 and ascertaining that this had no effect on the results of a trial computation.

All the results presented here are calculated with the phenomenological form factor F_F [Eqs. (13)–(15)] based on the Fermi distribution. Apart from the form factor, $d\sigma/dq^2$ is peaked inside the first diffraction minimum. This is just where the form factors F_F is less than both $F_{\rm I}$ and $F_{\rm II}$. Thus our results for the total cross sections are some 10% smaller than those of CSW based on their form factor $F_{\rm II}$.[17]

As is apparent from Figs. 7–14 and Table I, the transverse momenta of final charged leptons are disappointingly large, of the same order of magnitude as for strong interactions. The widths of p_t distributions increase with energy; yet those of $\Delta p_\parallel$ do not, even decreasing slightly.

This behavior may perhaps be understood, in a very rough fashion. We have seen that the q^2 behavior dominates. We can express q^2 as

$$q^2 \approx |\vec{q}|^2 = (\vec{p}_{\perp 2}+\vec{p}_{\perp 3}+\vec{p}_{\perp 4})^2 + (\Delta p_{\parallel 2}+\Delta p_{\parallel 3}+\Delta p_{\parallel 4}+\epsilon)^2 ,$$
$$\epsilon = \epsilon_1 - |\vec{p}_2| - |\vec{p}_3| - |\vec{p}_4| \approx m_4^2/2\epsilon_4 + m_3^2/2\epsilon_3 , \qquad (31)$$

where $\vec{p}_{\perp i}$ are the transverse momenta of the final leptons. One has the strict inequalities

$$\Delta p_\parallel < |\vec{q}| ,$$
$$p_\perp \approx p_t = (2p\Delta p_\parallel)^{1/2} < (2p|\vec{q}|)^{1/2} . \qquad (32)$$

Phase space, however, favors large $\vec{p}_\perp$, which are best attained for given q^2 if $\vec{p}_{\perp 2}+\vec{p}_{\perp 3}+\vec{p}_{\perp 4}$ in (31)

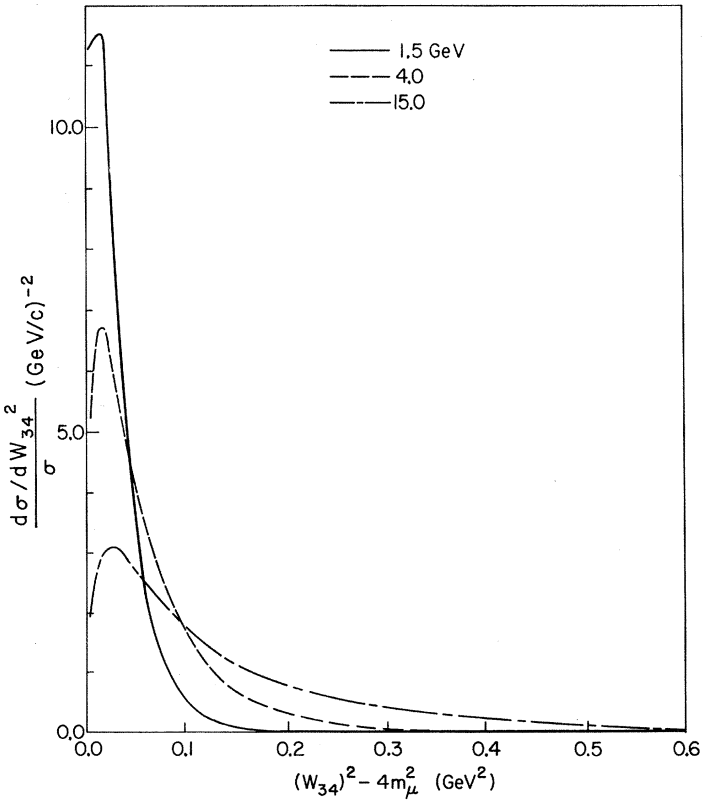

FIG. 16. Distributions in invariant mass-squared $W_{34}^2 = -(p_3+p_4)^2$ of charged leptons from coherent process (a) off ^{208}Pb target.

cancels down to terms of order $\Delta p_{\parallel}$. One may then expect to see the $\Delta p_{\parallel}$ upper limit in (32) be attained by average values of $\Delta p_{\parallel}$, i.e., to see

$$\langle \Delta p_{\parallel} \rangle_{\rm av} \simeq \tfrac{1}{3} \langle |\vec{q}| \rangle_{\rm av} ,$$
$$\langle p_t \rangle_{\rm av} \simeq (\tfrac{2}{3} \langle p \rangle_{\rm av} \langle |\vec{q}| \rangle_{\rm av})^{1/2} . \quad (33)$$

A look at Table I shows that these very rough equalities are satisfied within more or less constant factors of 5 and 3, respectively, for process (a); at least the trends in energy dependence of the widths of distributions in p_t and $\Delta p_{\parallel}$ are correctly given. Of course this reasoning is very loose, and wholly inadequate when the charged leptons are different in mass.

The Fermi interaction processes we consider will probably never be a serious background for W production, if the intermediate boson exists in a form close to what has been proposed. If one is right at threshold, the characteristic distribution for the transverse momentum of the final positive lepton will be broader than for the production mode considered here, although this lepton is emitted preferentially backwards in the W center-of-mass system due to polarization effects connected to helicity conservation. If one is well above threshold, then, since W production is a semi-weak process, its cross section is much larger than the cross sections we have been considering here (which then corresponds to an intermediate virtual W) and more detailed comparative calculations would have to be done to see to what extent they can be distinguished from the real "background."

The separation of the two-muon process (a) from process (7), where one has an intermediate π^+ may turn out to be very difficult, both because the transverse momenta in process (1), (a) are large and because the μ^+ carries away a relatively small fraction of the total available energy, down to 16% at 40 GeV.

The pions will presumably come mostly from two different production modes, either via a nucleon resonance [Fig. 19 (a)] or through some diffractive process [Fig. 19 (b)]. In the first case, it is known from analysis of electron data by Walecka *et al.*[18,19] that

$$k^2 \equiv (p_\nu - p_{\mu^-})^2 = (p_N - p_{N^*})^2 \approx 2|\vec{p}_\nu||\vec{p}_{\mu^-}|(1 - \cos\theta_{\mu^-})$$

is limited by the nucleon form factors. The CERN

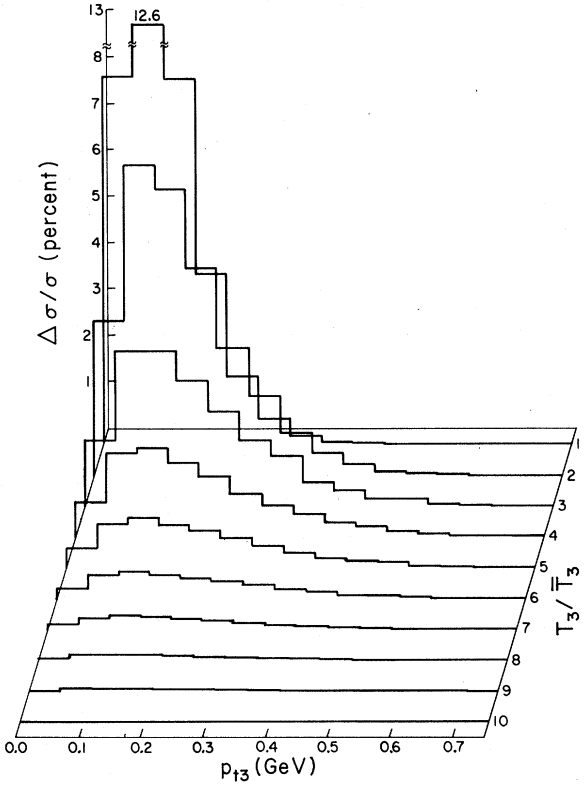

FIG. 17. Double distribution in transverse momentum p_{t3} versus kinetic energy T_3 of the μ^+ from coherent reaction (a) off ^{208}Pb at $\epsilon_1 = 15$ GeV. Each of the ten histograms (1–10 as labeled on the right and displayed with successively shifted origins) has fifteen bins. The height of the nth bin in the kth histogram gives the fraction $\Delta\sigma/\sigma$ of the events having $(k-1)/10 \leq T_3/\overline{T}_3 \leq k/10$ and $(n-1)\times(0.05\ \text{GeV}) \leq n \times (0.05\ \text{GeV})$.

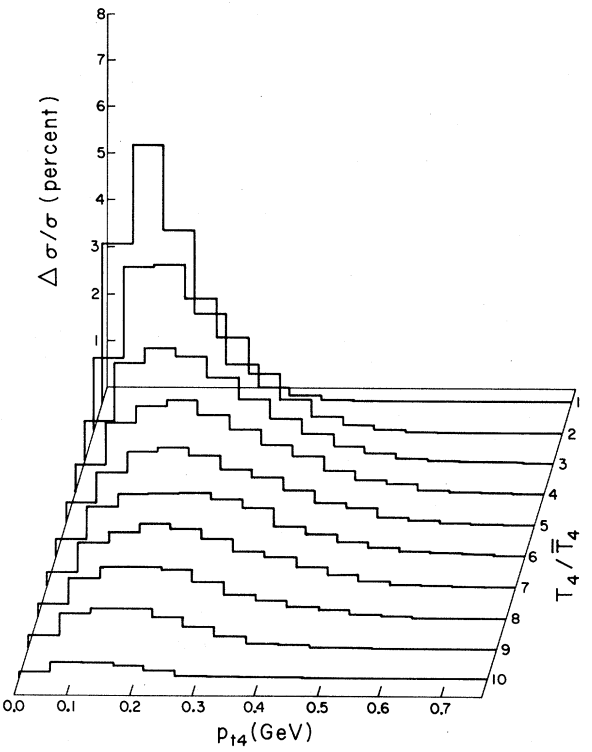

FIG. 18. Double distribution in transverse momentum p_{t4} versus kinetic energy T_4 of the μ^- from coherent reaction (a) of ^{208}Pb at $\epsilon_1 = 15$ GeV. Compare Fig. 19; the histogramming scheme is the same as here.

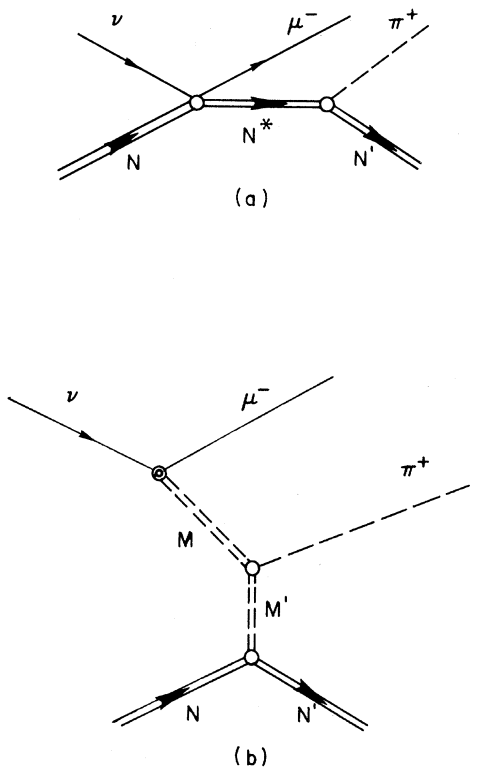

FIG. 19. Diagrams for experimental background to processes (1). (a) Resonant production. (b) Diffractive process. N and N' are single nucleon states, and N^* is a nucleon resonance.

experiments indicate the axial-vector form factor to be not very different from the vector ones, so that $k^2 < 1$ (GeV/c)^2. Purely from kinematics we know that

$$E_{\pi^+} < (k^2 + M^2 + M^{*2})(m_\pi{}^2 + M^{*2} - M^2)/2MM^{*2}, \tag{34}$$

where M^* is the mass of the resonance and M that of the nucleon. For the $\Delta(1236)$ one finds, putting $k^2 = 1$ (GeV/c)^2 into (34), that

$$E_{\pi^+} < 0.8 \text{ GeV}.$$

One has also, therefore,

$$p_{t\mu^-}{}^2 < k^2 \lesssim 1 (\text{GeV}/c)^2,$$

$$E_{\mu^+} < E_{\pi^+} \lesssim 0.8 \text{ GeV}.$$

This class of pions should therefore not be a very serious problem at NAL energies ($\epsilon_1 \simeq 15$ GeV), since a cut on E_{μ^+} at 1 GeV would eliminate nearly all of them, and only about 20% of the events (1), (a). Higher resonances decay mainly to multipion events, and peripheral or diffractive processes do not seem to be important at CERN energies. However, since the cross section for production of one pion is 10^5 to 10^6 times the cross section for process (a), it is clear that a careful experimental study of the one pion spectrum will have to be done with the same neutrino spectrum and the same target as one wants to use to detect the double muon process, (a) of Eq. (1).

To conclude, lepton triplets produced through the four-fermion interaction may not have the outstanding kinematical characteristics one could have hoped for. Nevertheless, we certainly feel that it is worthwhile to push experiments to detect them. They are still the best hope for observing diagonal weak interactions and virtual weak interactions in processes for which the predictions of weak-interaction theory may be calculated to arbitrary accuracy independent of strong-interaction models.

ACKNOWLEDGMENTS

We are indebted to Professor J. D. Walecka for suggesting this work and for constant advice and encouragement. One of the authors (J. L.) would like to thank Professor L. I. Schiff and Professor J. D. Walecka for the hospitality extended to him at the Institute of Theoretical Physics, Stanford University.

APPENDIX A

The results of completing the traces in (9) and carrying out the interesting contractions are

$$\begin{aligned}
2^{-8} P_\alpha L_{\alpha\beta} P_\beta = {} & (4P\cdot p_3 p_1\cdot q q\cdot P - M^2 q^2 p_1\cdot p_3 + 2M^2 q\cdot p_1 q\cdot p_3 - 2P\cdot p_3 q^2 p_1\cdot P) p_2\cdot p_4 D_3{}^{-2} \\
& + (4P\cdot p_4 p_2\cdot q q\cdot P - M^2 q^2 p_2\cdot p_4 + 2M^2 q\cdot p_2 q\cdot p_4 - 2P\cdot p_4 q^2 p_2\cdot P) p_1\cdot p_3 D_4{}^{-2} \\
& - D_3{}^{-1} D_4{}^{-1} [2M^2 (p_4\cdot q(p_2\cdot p_1 p_3\cdot q - p_2\cdot p_3 p_1\cdot q) - p_2\cdot q(p_4\cdot p_1 p_3\cdot q - p_4\cdot p_3 p_1\cdot q) \\
& + q^2 (p_2\cdot p_3 p_4\cdot p_1 - p_4\cdot p_3 p_2\cdot p_1)) - 2q\cdot P(p_4 p_2 q p_1 p_3 P) \\
& - 2q^2 (P\cdot p_4 p_2\cdot p_1 p_3\cdot P - P\cdot p_4 p_2\cdot p_3 p_1\cdot P - P\cdot p_3 p_1\cdot p_4 p_2\cdot P + P\cdot p_2 \quad p_4\cdot p_3 p_1\cdot P)] \\
& - 4[p_1\cdot p_3 (p_4\cdot P/D_4 - p_3\cdot P/D_3) + (p_1 p_3 P q)/D_3] \\
& \times [p_2\cdot p_4 (p_3\cdot P/D_3 - p_4\cdot P/D_4) + (p_2 p_4 P q)/D_4],
\end{aligned} \tag{A1}$$

$$2^{-9}L_{\alpha\alpha}=[2q\cdot p_2(m_4^2-q\cdot p_4)+p_2\cdot p_4(q^2-2m_4^2)]p_1\cdot p_3 D_4^{-2}+[2q\cdot p_1(m_3^2-q\cdot p_3)+p_1\cdot p_3(q^2-2m_3^2)]p_2\cdot p_4 D_3^{-2}$$
$$-D_3^{-1}D_4^{-1}[q^2(p_3p_1p_2p_4)+4p_2\cdot p_4 p_1\cdot p_3 p_3\cdot p_4-2p_2\cdot p_4(p_1p_3p_4q)-2p_1\cdot p_3(p_2p_4p_3q)]\,, \tag{A2}$$

where

$$D_{3,4}=q^2-2q\cdot p_{3,4}\,,$$

and we use the notations

$$(abcd)=\tfrac{1}{4}\mathrm{Tr}(\not a\not b\not c\not d)=a\cdot bc\cdot d-a\cdot cb\cdot d+a\cdot db\cdot c\,,$$

$$(p_4p_2qp_1p_3P)=\tfrac{1}{4}\mathrm{Tr}(\not p_4\not p_2\not q\not p_1\not p_3\not P)$$
$$=2p_2\cdot p_4(p_4p_1p_3P)+2p_1\cdot p_3(p_4p_2p_3P)+m_4^2(p_2p_1p_3P)+m_3^2(p_4p_2p_1P)\,.$$

This last may be found only after substituting four-momentum conservation, $q=p_2+p_3+p_4-p_1$.

The left-hand side of (A1) can be made to yield the general symmetric element of $L_{\alpha\beta}$, $\frac{1}{2}(L_{\alpha\beta}+L_{\beta\alpha})$, by replacing each M^2 by $-\delta_{\alpha\beta}$ and each pair of dot products $P\cdot ab\cdot P$ ($a,b=p_2,p_3,p_4,p_1,q$) by $\frac{1}{2}(a_\alpha b_\beta+a_\beta b_\alpha)$.

APPENDIX B

We shall begin by introducing a complete set of Lorentz invariants for the processes (1), (a)–(d). Taking four-momentum conservation into account, there are five independently varying vectors, giving ten dot products. One constraint equation comes from the mass restriction on the sixth four-vector and one from the requirement that the five four-vectors must be linearly dependent. The second constraint equation is unwieldy and impractical to use so we have described everything in terms of the nine invariants:

$$\begin{aligned}
x_0&=-p_1\cdot P=M\epsilon_1\,,\\
x_1&=q^2\,,\\
x_2&=-q\cdot p_1\,,\\
x_3&=-q\cdot p_3\,,\\
x_4&=-q\cdot p_4\,,\\
x_5&=-p_1\cdot p_3\,,\\
x_6&=-p_1\cdot p_4\,,\\
x_7&=-p_3\cdot P\,,\\
x_8&=-p_4\cdot P\,.
\end{aligned} \tag{B1}$$

All other relevant invariants are scalar products which may be expressed in terms of x_1–x_8:

$$\begin{aligned}
P\cdot q&=\tfrac{1}{2}x_1\,,\\
P\cdot p_2&=\tfrac{1}{2}x_1-x_0+x_7+x_8\,,\\
q\cdot p_2&=x_1-x_2+x_3+x_4\,,\\
p_1\cdot p_2&=-x_2+x_5+x_6\,,\\
p_2\cdot p_3&=\tfrac{1}{2}(m_3^2-m_4^2+x_1)-x_2+x_4+x_6\,,\\
p_2\cdot p_4&=\tfrac{1}{2}(m_4^2-m_3^2+x_1)-x_2+x_3+x_5\,,\\
p_3\cdot p_4&=\tfrac{1}{2}(m_4^2+m_3^2-x_1)+x_2-x_3-x_4-x_5-x_6\,.
\end{aligned} \tag{B2}$$

We then have the problems of relating the integration (8) to those in (21) (i.e., giving J) and expressing $x_1,x_2,\ldots,x_8$ in terms of $u_1,u_2,\ldots,u_7$ (x_0 being already fixed as $M\epsilon_1$). Most of the latter task is already done by (24). We now proceed to do the integrations in (8) from the outside inwards.

One integrates $d^3P'/2E'$ in the center-of-mass frame A defined by $\vec{p}_1+\vec{P}=0$. With $\vec{P}$ defining the z axis, the azimuthal integration is trivial and one gets [see CSW, Appendix B, (B.23)]

$$d^3P'/2E'=2\pi dx_1dx_2/4M\epsilon_1$$
$$=2\pi[8M\epsilon_1F^2(x_1)]^{-1}du_1du_2\,, \tag{B3}$$

where, from (24),

$$u_1=\int_{x_1}^{\infty}F^2(x)dx\,,$$

$$u_2=2x_2-x_1-(m_3+m_4)^2\,.$$

The limits $\bar{u}_1$ and $\underline{u}_1$ are given implicitly by the limits of x_1 [after CSW (B.27)]:

$$\left.\begin{matrix}\bar{x}_1\\ \underline{x}_1\end{matrix}\right\}=\frac{2\epsilon_1^2}{1+2g}\left\{1-\frac{m_L^2}{2\epsilon_1^2}(1+g)\pm\left[\left(1-\frac{m_L^2}{2\epsilon_1^2}(1+g)\right)^2-\frac{m_L^4}{4\epsilon_1^4}(1+2g)\right]^{1/2}\right\}, \tag{B4}$$

$$\underline{x}_1=m_L^4\bar{x}_1^{-1}(1+2g)^{-1}\,,$$

with $g=\epsilon_1/M$ and $m_L=m_3+m_4$. The second equation follows from the first, but, in numerical computations, its use avoids the necessity of subtracting two large numbers (of order unity) to obtain a very small result (of order m_L^4/ϵ_1^4). The limits on u_2 are derivable directly from CSW's Eqs. (B.24) and (B.26) as

$$\begin{aligned}
\underline{u}_2&=0\,,\\
\bar{u}_2&=\tfrac{1}{2}(\bar{x}_2+x_1)=\frac{(1+2g)(\bar{x}_1-x_1)(x_1-\underline{x}_1)}{m_L^2+x_1(1+g)+2\epsilon_1(x_1+x_1^2/4M^2)^{1/2}}\,.
\end{aligned} \tag{B5}$$

The first equality comes from the fact that $W_B^2 \equiv 2x_2 - x_1 = -(p_1+q)^2$ is the available energy squared in the three-lepton center-of-mass frame and must be at least m_L^2. The second is more complicated algebraically than direct application of CSW would give, but, like the second equation in (B4), it is better for use in numerical calculations, since, for x_1 near its limits, the alternative expressions involve subtraction of large numbers to obtain a very small result. [Still another example of this phenomenon is the reason u_2 was used as an integration variable as opposed to x_2: $2x_2 - x_1$, which may be as small as m_L^2, is the difference of numbers as large as ϵ_1^2 or M^2; therefore it is better to calculate $x_2 = \frac{1}{2}(u_2 + m_L^2 + x_1)$ than to calculate $W_B^2 = 2x_2 - x_1$ from x_2.]

The integral $d^3p_3/2\epsilon_3$, with P' now regarded as fixed, is done in the frame B defined by $\vec{p}_1 + \vec{q} = 0$. If $\vec{q}$ is taken to define the z axis and $\vec{P}$ to lie in the yz plane, one has

$$x_3 = q_0^B \epsilon_3^B - |\vec{q}|^B |\vec{p}_3|^B \cos\theta_3 , \tag{B6a}$$

$$x_5 = \epsilon_1^B \epsilon_3^B + \epsilon_1^B |\vec{p}_3|^B \cos\theta_3 , \tag{B6b}$$

$$x_7 = P_0^B \epsilon_3^B - |\vec{P}|^B |\vec{p}_3|^B (\cos\theta_3 \cos\theta_P + \cos\varphi_3 \sin\theta_3 \sin\theta_P) , \tag{B6c}$$

where θ_P is the angle between $\vec{P}$ and $\vec{q}$. Using (B6a) and (B6b), and finally (24) one has

$$d^3p_3/2\epsilon_3 = dx_3 dx_5 d\varphi_3/2x_2 = D_3(16x_2 u_4^{1/2})^{-1} du_3 du_4 du_5 , \tag{B7}$$

where

$$x_3 = \tfrac{1}{2}(D_3 - x_1) = \tfrac{1}{2}(e^{u_3} - x_1) ,$$
$$x_5 = x_2 - x_3 - \tfrac{1}{2}(m_4^2 - m_3^2 + x_1 + u_4^{1/2}) . \tag{B8}$$

The kinematically allowed region in x_3 and x_5 is bounded by the curves [CSW and (B17) and (B18)]

$$x_5(2x_2 x_3 + x_1 x_5) = m_3^2 x_2^2 ,$$
$$W_c^2 \equiv 2x_2 - x_1 - 2x_3 - 2x_5 + m_3^2 = m_4^2 ,$$

from which limits on u_3 and u_4 are straightforwardly derived:

$$\bar{u}_3 = \ln \bar{D}_3 , \quad \underline{u}_3 = \ln \underline{D}_3 , \tag{B9a}$$

where

$$\left.\begin{matrix}\bar{D}_3 \\ \underline{D}_3\end{matrix}\right\} = m_3^2 + x_1 m_4^2/W_B^2 + x_2 y_\pm / W_B^2 ,$$

$$y_\pm = (W_B^2 - m_3^2 - m_4^2) \pm [(W_B^2 - m_3^2 - m_4^2)^2 - 4m_3^2 m_4^2]^{1/2} , \tag{B9b}$$

$$y_- = 4m_3^2 m_4^2 / y_+ ,$$

and

$$\underline{u}_4 = 0 , \tag{B10}$$

$$\bar{u}_4 = \frac{(\bar{D}_3 - D_3)(D_3 - \underline{D}_3) W_B^2/x_1}{u_2 + 2m_3 m_L + 2x_3(x_2 - x_1)/x_1 + 2x_2(x_3^2 + m_3^2 x_1)^{1/2}/x_1} .$$

The limits on u_5 are, of course,

$$\bar{u}_5 = 2\pi , \qquad \underline{u}_5 = 0 . \tag{B11}$$

In practice we have picked our random points $\{u\}$ from only half the range of u_5, i.e., $0 \leq u_5 \leq \pi$. This makes no difference as everything is invariant under u_5 going to $2\pi - u_5$ (unless one wishes, as we have not, to obtain distributions in a variable which is not invariant under mirror reflection). Equation (B6c), upon substitution of

$$P_0^B = -P\cdot(p_1+q)/W_B = (x_0 - \tfrac{1}{2}x_1)/W_B ,$$
$$|\vec{P}|^B = [(P_0^B)^2 - M^2]^{1/2} ,$$
$$\epsilon_3^B = -p_3\cdot(p_1+q)/W_B = (x_5 + x_3)/W_B ,$$
$$|\vec{p}_3|^B = [(\epsilon_3^B)^2 - m_3^2]^{1/2} ,$$
$$q_0^B = -q\cdot(p_1+q)/W_B = (x_2 - x_1)/W_B ,$$
$$|\vec{q}|^B = [(q_0^B)^2 + x_1]^{1/2} ,$$
$$\cos\theta_P = (P_0^B q_0^B + \tfrac{1}{2}x_1)/|\vec{P}|^B |\vec{q}|^B ,$$

becomes, after some algebra,

$$x_7 = (x_0 x_1 x_5 + x_0 x_2 x_3 - \tfrac{1}{2}x_1 x_2 x_5) x_2^{-2} - (P_2 P_5)^{1/2} \cos\varphi_3 , \tag{B12}$$

where

$$P_2 = M^2 \tfrac{1}{2}(\bar{u}_2 - u_2) \times [x_2 + \epsilon_1 x_1/2M + \epsilon_1(x_1 + x_1^2/4M^2)^{1/2}] x_2^{-2} ,$$
$$P_5 = x_1 \tfrac{1}{2}(\sqrt{\bar{u}_4} - \sqrt{u_4}) \times [\tfrac{1}{2}(\sqrt{\bar{u}_4} - \sqrt{u_4}) + 2x_2(x_3^2 + m_3^2 x_1)^{1/2}/x_1] x_2^{-2} . \tag{B13}$$

We finally evaluate the integrals

$$\int \frac{d^3\vec{p}_2}{2\epsilon_2} \frac{d^3\vec{p}_4}{2\epsilon_4} \delta^4(q + p_1 - p_2 - p_3 - p_4)$$

in the frame C defined by $\vec{p}_1 + \vec{q} - \vec{p}_3 = 0$. One takes $\vec{q}$ to define the z direction and orients the axes so that $\vec{p}_1$ is in the yz plane. Following CSW in doing four of the integrations against the δ functions, one gets the two-dimensional integral [CSW (B10)]

$$\int\int\int\int \frac{d^3\vec{p}_4}{2\epsilon_4} \frac{d^3\vec{p}_2}{2\epsilon_2} \delta^4(q + p_1 - p_2 - p_3 - p_4) = (4|\vec{q}|^C W_C)^{-1} dx_4 d\varphi_4 = D_4(8|\vec{q}|^C W_C)^{-1} du_6 du_7 , \tag{B14}$$

where, by (24),

$$x_4 = \tfrac{1}{2}(D_4 - x_1) = \tfrac{1}{2}(-x_1 + e^{u_6}),$$
$$\varphi_4 = u_7 . \tag{B15}$$

In (B14) $|\vec{q}|^C$ is the magnitude of the three-vector $\vec{q}$ in this frame C, given by

$$|\vec{q}|^C W_C = [(x_2 - x_3)^2 - 2x_1x_5 + m_3^2 x_1]^{1/2} . \tag{B16}$$

The upper and lower limits are given by

$$\bar{u}_7 = 2\pi , \quad \underline{u}_7 = 0 ,$$
$$\bar{u}_6 = \ln \bar{D}_4 , \quad \underline{u}_6 = \ln \underline{D}_4 , \tag{B17}$$

where

$$\left.\begin{matrix}\bar{D}_4 \\ \underline{D}_4\end{matrix}\right\} = m_4^2(W_C^2 + 2x_5 - m_3^2)W_C^{-2} + \tfrac{1}{2}(1 - m_4^2/W_C^2)$$
$$\times \{W_C^2 + x_1 + 2x_5 - m_3^2 \pm [(W_C^2 + 2x_5 + x_1 - m_3^2)^2 - 4x_1(2x_5 - m_3^2)]^{1/2}\} , \tag{B18}$$

but in practice $\underline{D}_4$ is calculated from

$$\underline{D}_4 = m_4^2(W_C^2 + 2x_5 - m_3^2)W_C^{-2} + 2(1 - m_4^2/W_C^2)$$
$$\times x_1(2x_5 - m_3^2)\{(W_C^2 + x_1 + 2x_5 - m_3^2) + [(W_C^2 + x_1 + 2x_5 - m_3^2)^2 - 4x_1(2x_5 - m_3^2)]^{1/2}\}^{-1} \tag{B19}$$

in order that the numerical calculation be free of situations where two large numbers subtract to give a small result. (B18) and (B19) are algebraically equivalent to CSW's (B11) and are derived therefrom.

One then expresses x_6 and x_8 in terms of x_4 and φ_4 by

$$x_6 = \epsilon_1^C \epsilon_4^C - \epsilon_1^C |\vec{p}_4|^C (\cos\theta_4 \cos\theta_{\vec{p}_1\vec{q}} + \sin\theta_4 \sin\theta_{\vec{p}_1\vec{q}} \cos\varphi_4) ,$$
$$x_8 = P_0^C \epsilon_4^C - |\vec{P}|^C |\vec{p}_4|^C [\cos\theta_4 \cos\theta_{\vec{P}\vec{q}} + \sin\theta_4 \sin\theta_{\vec{P}\vec{q}} \cos(\varphi_4 - \Phi)] . \tag{B20}$$

$\theta_{\vec{p}_1\vec{q}}$ is the angle between vectors $\vec{p}_1$ and $\vec{q}$ in the C frame; $\theta_{\vec{P}\vec{q}}$ is similarly defined; θ_4 is $\theta_{\vec{p}_4\vec{q}}$; Φ is the azimuthal angle of P. Defining the quantities in the C frame:

$$P_0^C = (x_0 - \tfrac{1}{2}x_1 - x_7/W_C) , \quad |\vec{P}|^C = [(P_0^C)^2 - M^2]^{1/2} ,$$
$$q_0^C = (x_2 - x_1 - x_3)/W_C , \quad |\vec{q}|^C = [(q_0^C)^2 + x_1]^{1/2} ,$$
$$\epsilon_1^C = (x_2 - x_5)/W_C ,$$
$$\epsilon_4^C = (W_C^2 + m_4^2)/2W_C ,$$
$$|\vec{p}_4|^C = (W_C^2 - m_4^2)/2W_C = u_4^{1/2}/2W_C ,$$
$$\cos\theta_4 = (\epsilon_4^C q_0^C - x_4)/|\vec{p}_4|^C |\vec{q}|^C ,$$
$$\cos\theta_{\vec{P}\vec{q}} = (P_0^C q_0^C + \tfrac{1}{2}x_1)/|\vec{P}|^C |\vec{q}|^C ,$$
$$\cos\theta_{\vec{p}_1\vec{q}} = (\epsilon_1^C q_0^C - x_2)/\epsilon_1^C |\vec{q}|^C ,$$
$$\cos\theta_{\vec{P}\vec{p}_1} = (P_0^C \epsilon_1^C - x_0)/\epsilon_1^C |\vec{P}|^C ,$$
$$\cos\Phi = \frac{\cos\theta_{\vec{P}\vec{p}_1} - \cos\theta_{\vec{P}\vec{q}} \cos\theta_{\vec{p}_1\vec{q}}}{\sin\theta_{\vec{P}\vec{q}} \sin\theta_{\vec{p}_1\vec{q}}} ,$$

and substituting into (B20) one eventually gets

$$x_6 = \{\tfrac{1}{2}(W_C^2 + m_4^2)[x_2(x_2 - x_3) - x_1x_5] + x_4(x_2 - x_5)(x_2 - x_1 - x_3) - x_4x_2W_C^2\}(|\vec{q}|^C W_C)^{-2} - x_2(P_4P_5)^{1/2}(\cos\varphi_4)/|\vec{q}|^C W_C ,$$
$$x_8 = \{\tfrac{1}{2}(W_C^2 + m_4^2)x_1[x_0 - x_7 - \tfrac{1}{2}(x_2 - x_3)] + x_4(x_0 - x_7)(x_2 - x_1 - x_3) + \tfrac{1}{2}x_1x_4(x_2 - x_3 - 2x_5 + m_3^2)\} \times (|\vec{q}|^C W_C)^{-2} - (P_2P_4)^{1/2}\sin u_5 \sin\varphi_4 - P_4^{1/2}[(x_2 - x_3 - x_1x_5/x_2) \times P_2^{1/2}\cos u_5 + x_1(x_0 - \tfrac{1}{2}x_2)P_5^{1/2}/x_2]/W_C|\vec{q}|^C , \tag{B21}$$

where

$$P_4 = (\bar{D}_4 - D_4)(D_4 - \underline{D}_4)/4(|\vec{q}|^C)^2 .$$

Finally, we combine (B3), (B7), and (B14) to get (27).

---

*Research sponsored by the Air Force Office of Scientific Research, Office of Aerospace Research, U. S. Air Force, under AFOSR Contract No. F44620-68-C-0075.

†NTNF Fellow on leave from University of Trondheim, Norges Laererhøgskole, Norway (present address).

‡National Science Foundation Predoctoral Fellow.

[1]W. Czyz, G. C. Sheppey, and J. D. Walecka, Nuovo Cimento 34, 404 (1964), hereafter referred to as CSW. They also give references to earlier work.

[2]M. Gell-Mann, M. L. Goldberger, N. M. Kroll, and F. E. Low, Phys. Rev. 179, 1518 (1968).

[3]D. H. Perkins, in *Topical Conference on Weak Interactions, CERN, Geneva, Switzerland, 1969* (CERN, Geneva, 1969), pp. 1–42.

[4]R. B. Stothers, Phys. Rev. Letters 24, 538 (1970).

[5]T. D. Lee, P. Markstein, and C. N. Yang, Phys. Rev. Letters 7, 429 (1961).

[6]J. S. Bell and M. Veltman, Phys. Letters 5, 94 (1963).

[7]R. W. Brown and J. Smith, Phys. Rev. D 3, 207 (1971), give calculations at energies pertinent to the search for the W at NAL.

[8]C. Baltay and H. Wachsmuth, Aspen Summer Study

Report No. SS-133 (unpublished).
[9]For a review, see C. Franzinetti, in *Topical Conference on Weak Interactions, CERN, Geneva, Switzerland, 1969*, Ref. 3, pp. 43–60.
[10]The Fierz transformation is not an essential element of the calculation. However, it does simplify the algebra.
[11]See, e.g., R. E. Taylor, in *Proceedings of the Third International Symposium on Electron and Photon Interactions at High Energies, Stanford Linear Accelerator Center, Stanford, California, 1967* (Clearing House of Federal Scientific and Technical Information, Washington, D.C., 1968), pp. 78–100. The neutron electric form factor may not be precisely zero, but even G_E (neutron) $\propto xG$ would add no more than 10% to the total neutron cross sections at 15 GeV.
[12]R. Hofstadter and H. R. Collard, in Landolt-Börnstein, *Numerical Data and Functional Relationships in Science and Technology* (Springer-Verlag, Berlin, 1967), Vol. I/2, p. 26.
[13]I. Sick and J. S. McCarthy, Nucl. Phys. A150, 631 (1970).
[14]J. S. R. Chisholm, Nuovo Cimento 30, 426 (1963).
[15]Reference 6. The value 235 F is a representative one, somewhat low for the heavier nuclei – see E. J. Moniz, Phys. Rev. 184, 1154 (1969).
[16]See, e.g., the discussion in J. S. Bell and C. H. Llewellyn Smith, CERN Report No. CERN-TH-1259 (unpublished).
[17]For ^{12}C there is an additional 30% reduction coming from the discrepancy between $a = 0.93A^{1/3}$, which CSW used, and $a = (0.58 + 0.82A^{1/3})$, which gives low-q correspondence with F_F.
[18]J. D. Walecka and P. Zucker, Phys. Rev. 167, 1479 (1968).
[19]P. Pritchett and P. Zucker, Phys. Rev. D 1, 175 (1970).

PHYSICAL REVIEW D VOLUME 3, NUMBER 11 1 JUNE 1971

Current Matrix Elements from a Relativistic Quark Model*

R. P. Feynman, M. Kislinger, and F. Ravndal
Lauritsen Laboratory of Physics, California Institute of Technology, Pasadena, California 91109
(Received 17 December 1970)

A relativistic equation to represent the symmetric quark model of hadrons with harmonic interaction is used to define and calculate matrix elements of vector and axial-vector currents. Elements between states with large mass differences are too big compared to experiment, so a factor whose functional form involves one arbitrary constant is introduced to compensate this. The vector elements are compared with experiments on photoelectric meson production, K_{l3} decay, and $\omega \to \pi\gamma$. Pseudoscalar-meson decay widths of hadrons are calculated supposing the amplitude is proportional (with one new scale constant) to the divergence of the axial-vector current matrix elements. Starting only from these two constants, the slope of the Regge trajectories, and the masses of the particles, 75 matrix elements are calculated, of which more than $\frac{3}{4}$ agree with the experimental values within 40%. The problems of extending this calculational scheme to a viable physical theory are discussed.

INTRODUCTION

The symmetric, nonrelativistic harmonic-oscillator quark model has been shown by a number of people[1,2] to offer considerable promise of helping to organize the wealth of data in the resonance region for high-energy phenomena. We intend here to bring some of these results together in a unified method of calculation in order to judge better the validity of this organizing power.

A truly relativistic quantum-mechanical theory today seems available only in the complexities of field theory with its many virtual states involving, for example, pairs, etc. It is so complex that no particular dynamic regularities among the resonances are expected of it, other than those resulting from symmetries of the original Hamiltonian. We have gone in a different direction, sacrificing theoretical adequacy for simplicity. We shall choose a relativistic theory which is naive and obviously wrong in its simplicity, but which is definite and in which we can calculate as many things as possible – not expecting the results to agree exactly with experiment, but to see how closely our "shadow of the truth" equation gives a partial reflection of reality. In our attempt to maintain simplicity, we shall evidently have to violate known principles of a complete relativistic field theory (for example, unitarity). We shall attempt to modify our calculated results in a general way to allow, in a vague way, for these errors.

This is, of course, quite dangerous – because if one allows too much latitude in modifying the results of the calculations, especially if empirical results are allowed to influence strongly the many arbitrary choices, the significance of later par-